Two-Photon Absorption in Near-IR Conjugated Molecules: Design Strategy and Structure–Property Relations

Olga V. Przhonska, Scott Webster, Lazaro A. Padilha, Honghua Hu, Alexey D. Kachkovski, David J. Hagan, and Eric W. Van Stryland

Abstract In the past few years, applications built around two-photon absorption (2PA) have emerged, which require new materials to be designed and characterized in order to discover new applications and to advance the existing ones. This chapter describes the nonlinear optical processes and characterization techniques along with design strategies and structure–property relations of cyanine and cyanine-like molecular structures with the goal of enhancing 2PA in the near-IR for multiphoton fluorescence sensing applications. Specifically, a detailed analysis of the linear and nonlinear optical properties of several classes of polymethine dyes, which include symmetrical and asymmetrical combinations of π-conjugated bridges with electron donating (D) or electron accepting (A) terminal groups, are presented. These structures are: D–π–D, A–π–A, D–π–A, and a quadrupolar type arrangement of D–π–A–π–D.

The results of this research combined with the growing literature on structure–property relations in organic materials is moving us closer to the ultimate goal of developing a predictive capability for the nonlinear optical properties of molecules.

Keywords Cyanine dyes · Excited state absorption · Polymethine dyes · Pump-probe · Two-photon absorption · Z-scan

O.V. Przhonska (✉)
Institute of Physics, National Academy of Sciences of Ukraine, Prospect Nauki 46, 03028, Kyiv, Ukraine
CREOL, the College of Optics and Photonics, University of Central Florida, Orlando, FL, USA
e-mail: olga@creol.ucf.edu
S. Webster, L.A. Padilha, H. Hu, D.J. Hagan, and E.W.V. Van Stryland
CREOL, the College of Optics and Photonics, University of Central Florida, Orlando, FL, USA
A.D. Kachkovski
Institute of Organic Chemistry, National Academy of Sciences, Kyiv, Ukraine

A.P. Demchenko (ed.), *Advanced Fluorescence Reporters in Chemistry and Biology I: Fundamentals and Molecular Design*, Springer Ser Fluoresc (2010) 8: 105–148,
DOI 10.1007/978-3-642-04702-2_4,

Contents

1 Introduction

Significant effort in the past decade has been given to the development of organic molecules and semiconductor quantum dots with large two-photon absorption (2PA) for applications in fluorescence sensing and biological imaging. Advances in several areas, including molecular and synthetic chemical designs, understanding of structure–property relations, and the wide availability of tunable femtosecond sources have enabled the development and discovery of molecules with larger 2PA cross sections, δ_{2PA}, and increased fluorescence quantum yields in the visible and near-infrared (NIR).

Organic molecules, with the capability of tailoring their linear and nonlinear optical properties by molecular structure modification, can be utilized in fluorescence sensing and biological imaging. Fluorescence imaging, where a dye molecule is attached to a particular component or species of a system under investigation, utilizes the difference in excitation energy and the emitted fluorophore's photon energy for increased signal to noise discrimination. This technique can be further enhanced by utilizing nonlinear excitation processes such as 2PA, where the excitation photon energy is less than the energy gap of the fluorophore where there is no linear absorption. Figure 1a shows a schematic of frequency degenerate (both excitation photons having the same frequency) 2PA (1) into the first allowed singlet state, (2) above the first allowed singlet state, and (3) a near double resonant condition, with a small intermediate state resonance, Δ, and a transition into an allowed final 2PA state.

Since 2PA is a third-order nonlinear susceptibility, $\chi^{(3)}$, process, large irradiances are needed to excite fluorophores into their excited state. Typically, femtosecond lasers are used in conjunction with tight focusing geometries to produce these large irradiances, thereby restricting 2PA to the focal volume, which can be as small as femtoliters. The one-photon excitation density in the focal region is proportional to the light intensity, whereas the two-photon excitation density is

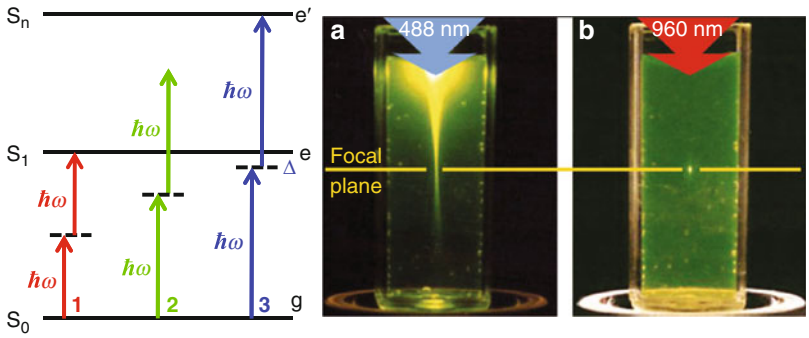

Fig. 1 (*Left*) Schematic of frequency degenerate 2PA (1) into the first allowed singlet state, (2) above the first allowed singlet state, and (3) a double resonant condition, with a small intermediate state resonance energy difference, Δ, and a transition into an allowed final 2PA state. (*Right*) Photograph illustrating the much sharper contrast of two-photon (**b**) versus one-photon excitation (**a**) (taken from [2])

proportional to the square of the irradiance and therefore falls rapidly away from the focus allowing decreased scattering. The 2PA review by M. Pawlicki et al [1] details the advantages and disadvantages of excitation by one- and two-photons. Figure 1b is a photograph of a cell containing a fluorophore that is excited with one-photon absorption (1PA) and 2PA, which illustrates the much sharper contrast in the excitation density for 2PA (taken from [2]).

Since the excitation wavelength is also less than the main transition energy, and usually in the NIR wavelength region, 2PA excitation is less likely to cause photochemical decomposition and decreases scattering due to longer wavelengths, thereby allowing applications involving in vivo imaging due to the low absorption and scattering of tissue in this wavelength range allowing for deep tissue imaging (up to 1 mm in commercially available systems) with high spatial resolution. Many excellent reviews for multiphoton microscopy and related techniques and applications are available [3–11].

This chapter summarizes our current knowledge and understanding of linear π-conjugated systems for NIR dyes: cyanines and cyanine-like molecules for one- and multiphoton applications, with a focus on the intramolecular spectroscopic properties and dynamics and the experimental methodologies used to characterize these particular organic systems and others.

1.1 Brief Historical Account of Two-Photon Absorption and π-Conjugated Systems

In the 1930s, Maria Göppert-Mayer [12], theoretically predicted the process of an atom being raised to an excited state of energy equal to the sum of two simultaneously

absorbed photons [13], but it was not until 1961, shortly after the development of the laser, that the phenomenon was experimentally verified due to the large irradiances needed. With the development of pulsed lasers of decreasing pulse widths (nanosecond, picoseconds, and femtosecond pulse widths) and increasing output energies, larger peak irradiances were obtained in the 1980s and 1990s, and 2PA research grew leading to the development of two-photon induced fluorescence microscopy for enhanced imaging [14].

The many theoretical and experimental studies of 2PA in the past few decades have enabled a more complete understanding of molecular transitions. Selection rules for 2PA are different from those for 1PA, which has led to complementary spectroscopic techniques that are currently employed in discovering new structure–property relationships. Several reviews exist concerning the design, synthesis, and characterization of particular organic dyes [1, 15–19] with the desire to understand their structure–property relationships for 2PA-enabled applications such as 3D optical data storage [20, 21], multiphoton 3D microfabrication [22], imaging (both biological [23] and chemical [24] sensing), and two-photon photodynamic therapy [25–27]. This review focuses on describing the 1PA fluorescence, 2PA, and related linear and nonlinear optical properties in π-conjugated cyanine and cyanine-like molecules for applications involving two-photon fluorescence.

1.2 Nonlinear Mechanisms in π-Conjugated Molecules

To understand the response of materials upon light irradiation, we describe the macroscopic polarization P as a function of the electric field E as:

$$P = P^{(1)} + P^{(2)} + P^{(3)} + \ldots = \varepsilon_0(\chi^{(1)}E + \chi^{(2)}E^2 + \chi^{(3)}E^3 + \ldots), \qquad (1)$$

where ε_0 is the dielectric constant in vacuum, $P^{(n)}$ denotes the nth order of polarization, and $\chi^{(n)}$ is the nth order optical susceptibility; $\chi^{(1)}$ describes the linear optical properties of the material; $\chi^{(2)}$ represents the second harmonic generation, sum frequency generation, optical rectification, parametric generation, and electro-optic effect, etc.; and $\chi^{(3)}$ is connected with third harmonic generation, nonlinear refraction (higher orders of $\chi^{(n)}$ for odd n can also contribute to nonlinear refraction), 2PA, stimulated Raman or Brillouin scattering, and four wave mixing, etc.

1.2.1 Two-Photon Absorption

Frequency degenerate 2PA is a third order, $\chi^{(3)}$, nonlinear optical process whereby two photons of equal energy are simultaneously absorbed to raise a system into an excited state of energy equal to that of the sum of the two photons. The propagation

of light of irradiance I, through a material of thickness z with 1PA and 2PA is written as:

$$\frac{\mathrm{d}I}{\mathrm{d}z} = -\alpha_1 I - \alpha_2 I^2 - ..., \tag{2}$$

where α_1 and α_2 are the one- and two-photon absorption coefficients. Higher order nonlinear absorptions are not discussed here, but formulations for three- and multiphoton absorption can be found elsewhere [28]. In this brief review, we focus on degenerate 2PA, which corresponds to two photons of equal energy. Details concerning nondegenerate 2PA can be found elsewhere [29–32]. Degenerate 2PA at a specific frequency, ω, is proportional to the imaginary part of $\chi^{(3)}$, expressed in SI units as:

$$\alpha_2(\omega) = \frac{3\omega}{2n^2c^2\varepsilon_0}\mathrm{Im}\left(\chi^3(-\omega;\omega,-\omega,\omega)\right), \tag{3}$$

where n is the refractive index and c is the speed of light. To characterize the 2PA of individual molecules, we define the 2PA cross section, $\delta_{2\mathrm{PA}}(\omega)$, which is given in units of 1×10^{-50} cm^4 s photon^{-1} molecule^{-1}. This unit is called "Goppert-Mayer" or "GM" in honor of the author of [12]. $\delta_{2\mathrm{PA}}(\omega)$ for an individual molecule can be expressed in SI units by:

$$\delta_{2\mathrm{PA}}(\omega) = \frac{\hbar\omega\alpha_2}{N} = \frac{3\hbar\omega^2}{2n^2c^2\varepsilon_0 N}\mathrm{Im}\left(\chi^3(-\omega;\omega,-\omega,\omega)\right), \tag{4}$$

where N is the number of molecules per unit volume.

In this chapter, we will discuss a simple quantum mechanical approach to model 2PA in molecular systems since it provides an accurate and comprehensive picture of the physics involved in the interaction. In 1971, Orr and Ward used a sum-over-states (SOS) model based on perturbation theory to derive $\chi^{(3)}$ [33]. This methodology sums all transitions between the ground state, and all possible excited states. Fortunately, a complete sum over all states is not necessary for modeling 2PA. Often, even as few as three states can give good insight. Therefore, a three-state model is developed to simplify the SOS approach [34–36]. In this model, the ground state (g), excited state as intermediate state (e), and another higher-lying excited state as a final two-photon state (e'), are considered (see Fig. 1). Transitions between ground state and excited state (g, e), and transitions between two excited states (e, e') are one-photon allowed so that their transition dipole moments are not zero: $\mu_{ge}, \mu_{ee'} \neq 0$, while transitions between the ground state and the higher-lying excited state (g, e') are forbidden: $\mu_{ge'} = 0$. All of the resonance terms are kept and the antiresonance terms are omitted. Considering only degenerate 2PA of linearly

parallel polarized light, the third-order susceptibility tensor can be written in SI Units as:

$$\chi^{(3)}_{xxxx}(2PA) = \frac{2N}{3!\varepsilon_0}\left\{\begin{array}{ll} \frac{\mu^x_{ge}\Delta\mu^x\Delta\mu^x\mu^x_{eg}}{(\Omega_{eg}-\hbar\omega)(\Omega_{eg}-2\hbar\omega)(\Omega_{eg}-\hbar\omega)} & \text{D - term} \\ + \frac{\mu^x_{ge}\Delta\mu^x\Delta\mu^x\mu^x_{eg}}{(\Omega^*_{eg}-\hbar\omega)(\Omega_{eg}-2\hbar\omega)(\Omega_{eg}-\hbar\omega)} & \text{D - term} \\ + \frac{\mu^x_{ge}\bar{\mu}^x_{ee'}\bar{\mu}^x_{e'e}\mu^x_{eg}}{(\Omega_{eg}-\hbar\omega)(\Omega_{e'g}-2\hbar\omega)(\Omega_{eg}-\hbar\omega)} & \text{T - term} \\ + \frac{\mu^x_{ge}\bar{\mu}^x_{ee'}\bar{\mu}^x_{e'e}\mu^x_{eg}}{(\Omega^*_{eg}-\hbar\omega)(\Omega_{e'g}-2\hbar\omega)(\Omega_{eg}-\hbar\omega)} & \text{T - term} \end{array}\right\} - \frac{2N}{3!\varepsilon_0}\left\{\begin{array}{ll} \frac{\mu^x_{ge}\mu^x_{eg}\mu^x_{ge}\mu^x_{eg}}{(\Omega_{eg}-\hbar\omega)(\Omega_{eg}-\hbar\omega)(\Omega_{eg}-\hbar\omega)} & \text{N - term} \\ \frac{\mu^x_{ge}\mu^x_{eg}\mu^x_{ge}\mu^x_{eg}}{(\Omega_{eg}-\hbar\omega)(\Omega^*_{eg}-\hbar\omega)(\Omega_{eg}-\hbar\omega)} & \text{N - term} \end{array}\right\} \tag{5}$$

where Ω_{eg} is the energy difference between e and g states including the transition linewidth, Γ_{eg}: $\Omega_{eg} = \hbar\omega_{eg} - i\Gamma_{eg}, \Omega^*_{eg} = \hbar\omega_{eg} + i\Gamma_{eg}$; $\Delta\mu^x$ is the permanent dipole moment difference between the excited state e and ground state g : $\Delta\mu^x = \mu^x_{ee} - \mu^x_{gg}$.

The first two terms in (5) are called "D-terms" or "dipolar terms," which are nonzero only if $\Delta\mu^x \neq 0$. The two-photon resonance denominator, $(\Omega_{eg} - 2\hbar\omega)$, indicates that an electron is excited into the lower excited state e. If we consider a near resonance condition: $\hbar\omega = \hbar\omega_{eg}/2$, the imaginary part of the D-terms can be written in SI units as:

$$\mathrm{Im}\left(\chi^3(2PA)_{\text{D - term}}\right) = \frac{N\mu^2_{ge}\Delta\mu^2}{3!\varepsilon_0\Gamma_{eg}}\frac{\left(\hbar\omega_{eg}\right)^2}{\left[\left(\hbar\omega_{eg}/2\right)^2 + \Gamma^2_{eg}\right]^2} \tag{6}$$

If the molecules possess different excited state permanent and ground state permanent dipole moments, the D-terms can contribute to 2PA. Centrosymmetric molecules do not have permanent dipole moments in both ground and excited states, so their D-terms are zero.

The second two terms in (5) are called "T-terms" or "two-photon terms", which have $(\Omega_{e'g} - 2\hbar\omega)$ in the denominator corresponding to the excitation of an electron into the higher-lying excited state e'. If we consider a resonance condition where $\hbar\omega = \hbar\omega_{e'g}/2$ and assume that the transition linewidth is narrow, $\Gamma_{eg} << [\hbar(\omega_{eg} - \omega_{e'g}/2)]/2$, the imaginary part of the T-term can then be expressed in SI units as:

$$\mathrm{Im}[\chi^{(3)}_{xxxx}(2PA)_{\text{T - term}}] = \frac{4N\mu^2_{ge}\mu^2_{ee'}}{3!\varepsilon_0\Gamma_{e'g}}\frac{1}{\left(\hbar\omega_{eg} - \hbar\omega_{e'g}/2\right)^2}. \tag{7}$$

In both cases, μ_{ge} and $\Delta\mu$, as well as μ_{ge} and $\mu_{ee'}$ are assumed to be parallel to each other. If there is an angle θ between the corresponding dipole moments μ_{ge} and $\mu_{ee'}$, an effective excited state transition dipole moment $\mu^{\text{eff}}_{ee'}$ should be used instead

of $\mu_{ee'}$ [37]: $\mu_{ee'}^{\text{eff}} = \mu_{ee'}\left[(2\cos^2(\theta)+1)/3\right]^{1/2}$. In isotropic media such as a solution, all D- and T-terms are averaged over the random orientations and should be divided by a factor of 5 [38].

The last two terms in (5) are called "N" or "negative terms" that do not contribute to two-photon absorption when the incident photon energy is far below the 1PA edge. However, very close to the one-photon edge, the N-terms in (5) may negatively contribute to the 2PA. This term is sometimes referred to as "virtual saturation" since it turns into real saturation at frequencies on or very near to resonance (within the linewidth). In semiconductors, this term is usually referred to as the AC-Stark or quadratic Stark effect and physically represents the shifting of the energy level with large optical fields [29].

The 2PA cross section spectrum, $\delta_{2\text{PA}}(\omega)$, including D- and T- terms but assuming we are far enough below the 1PA edge to ignore the N terms, can be presented in SI units as [39, 40]:

$$\delta_{2\text{PA}}(\omega) = \frac{1}{5c^2\hbar n^2 \varepsilon_0^2} \frac{(\hbar\omega)^2}{(\hbar\omega_{eg} - \hbar\omega)^2 + \Gamma_{eg}{}^2} \times \left[\frac{|\mu_{eg}|^2 |\Delta\mu|^2 \Gamma_{eg}}{(\hbar\omega_{eg} - 2\hbar\omega)^2 + \Gamma_{eg}{}^2} + \frac{|\mu_{eg}|^2 |\mu_{ee'}|^2 \Gamma_{e'g}}{(\hbar\omega_{e'g} - 2\hbar\omega)^2 + \Gamma_{e'g}{}^2} \right]. \quad (8)$$

In practice, for linear π-conjugated molecules, the 2PA spectra typically consist of several 2PA bands, corresponding to several final states (e') and the same intermediate state (e). Analysis of (8) identifies the main spectroscopic parameters responsible for $\delta_{2\text{PA}}$ and formulates the following general trends in structure–property relations. As seen from (8), the main spectroscopic parameters are: change in the permanent dipole moment $\Delta\mu$; transition dipole moments μ_{ge}, $\mu_{ee'}$; angles between dipole moments; linewidth Γ, and detuning energies from intermediate and final states, $(\hbar\omega_{eg} - \hbar\omega)$ and $(\hbar\omega_{e'g} - 2\hbar\omega)$.

Factors that can enhance $\delta_{2\text{PA}}(\omega)$ are:

1. *Increasing the transition dipole moments.* In molecular design, this can be realized by increasing the π-conjugation length, or by introducing electron donor/acceptor groups. In noncentrosymmetric molecules, increasing the difference of the ground and excited state permanent dipole moments can also increase $\delta_{2\text{PA}}(\omega)$
2. *Maximizing resonance terms.* Decreasing the detuning energy between intermediate and ground states can significantly enhance $\delta_{2\text{PA}}(\omega)$. This effect is called intermediate state resonance enhancement (ISRE). This is illustrated in Fig. 1a and is discussed in detail in [32]. If the intermediate state is located halfway between ground state and final state, a "double resonance" condition can be achieved, which can lead to a dramatic enhancement of $\delta_{2\text{PA}}(\omega)$
3. *Reducing the linewidth of the lowest energy one-photon transition.* Minimizing Γ increases $\delta_{2\text{PA}}(\omega)$, which allows for photons to closely approach the 1PA edge without one-photon losses

Additional details for enhancing 2PA in linear cyanine-like molecules will be discussed in Sect. 3.

1.2.2 Excited State Absorption (ESA)

Understanding the role of ESA in nonlinear absorbing systems is important for: (1) determining correct 2PA cross sections, illustrated in Sect. 1.2.3 by decoupling ESA from 2PA; (2) gaining insight into the nature of transitions from intermediate to final states in 2PA spectra; (3) determining the nature of higher-lying excited states that are not physically accessible through 2PA measurements; and (4) determining the intermediate transition dipole moments that can be additionally calculated by quantum chemical methods. Unlike 2PA, which is a $\chi^{(3)}$ process, ESA is a cascaded first-order susceptibility process, $\chi^{(1)}$, where two photons are sequentially absorbed to take the molecule to one excited and then a final state. This requires that the first absorbed photon has an energy equal to or larger than the lowest molecular transition energy.

The physical mechanisms involved in absorption and emission by the molecule can be illustrated by the 5-level energy model based on a Jablonski diagram [41] in Fig. 2a. The system can be excited by one-photon into vibrational sublevels of the first excited state (S_1), followed by a rapid vibronic relaxation to the lowest level in the S_1 state. There are several competing processes to depopulate the S_1 state: spontaneous decay or stimulated emission to the ground state (S_0); excitation into the higher-lying excited state (S_n) by absorbing another photon; or intersystem crossing leading to population of the first triplet state (T_1).

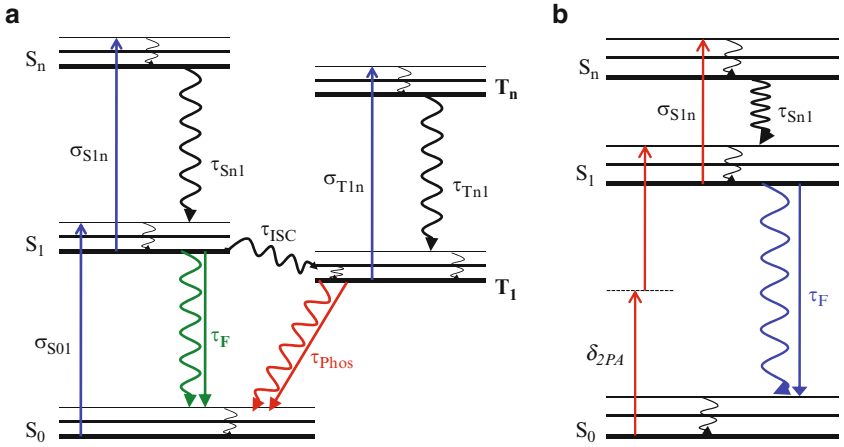

Fig. 2 (**a**) Energy level schematics for (**a**) a 5-level model including both singlet and triplet ESA and (**b**) 2PA-induced ESA, both including relaxation dynamics

Spontaneous decay from S_1 to S_0 can follow either a radiative pathway by emitting a photon (fluorescence), or a nonradiative pathway. The lifetime of the S_1 state is determined by the total decay rate of these two pathways, which is equal to the fluorescence lifetime τ_F. Stimulated emission occurs when there is spectral overlap between excitation and fluorescence; however, it may usually be neglected since excitation wavelengths are intentionally set out of the range of the fluorescence spectrum. ESA occurs when an S_1 electron absorbs another photon and is promoted to a higher lying state (S_n); if $\sigma_{S1n} > \sigma_{01}$, this is referred to as reverse saturable absorption (RSA). The decay rate from S_n to S_1 is normally much faster than the lifetime of the S_1 state ($\tau_{Sn1} << \tau_F$); so with small fluences (energy per area), the population of S_n can usually be assumed to be zero. But this approximation fails if the input fluence is very large, leading to significant population of the S_n state. In this case, another higher-lying singlet excited state $S_{n'}$ often needs to be included to take into account absorption from S_n to $S_{n'}$ (not shown in Fig. 2a). Intersystem crossing to the triplet state T_1 may occur when the excited electron undergoes a spin conversion, which is characterized by an intersystem crossing rate: $k_{ISC} = 1/\tau_{ISC}$. The decay from T_1 to S_0 can also follow a radiative pathway (phosphorescence) or nonradiative pathway; however, the lifetime of the T_1 state (τ_{Phos}) is long (usually 10^{-8} to 10^{2} s) due to its spin-forbidden nature. Therefore, provided the presence of a triplet state in the molecular system and long-duration input laser pulse widths are used (usually larger than nanoseconds, but possibly as small as picoseconds [42]), ESA absorption from T_1 to T_n should also be considered when modeling results.

To mathematically describe the physical processes indicated above, the following propagation and rate equations are introduced in the form of differential equations as:

$$\begin{aligned}
\frac{dI}{dz} &= -\sigma_{S01}N_0 I - \sigma_{S1n}N_{S1}I - \sigma_{T1n}N_{T1}I \\
\frac{dN_0}{dt} &= -\frac{\sigma_{S01}N_0 I}{\hbar\omega} + \frac{N_{S1}}{\tau_F} + \frac{N_{T1}}{\tau_{Phos}} \\
\frac{dN_{S1}}{dt} &= \frac{\sigma_{S01}N_0 I}{\hbar\omega} - \frac{N_{S1}}{\tau_F} - \frac{\sigma_{S1n}N_{S1}I}{\hbar\omega} + \frac{N_{Sn}}{\tau_{Sn1}} - \frac{N_{S1}}{\tau_{ISC}} \\
\frac{dN_{Sn}}{dt} &= \frac{\sigma_{S1n}N_{S1}I}{\hbar\omega} - \frac{N_{Sn}}{\tau_{Sn1}} \\
\frac{dN_{T1}}{dt} &= -\frac{\sigma_{T1n}N_{T1}I}{\hbar\omega} + \frac{N_{Tn}}{\tau_{Tn1}} + \frac{N_{S1}}{\tau_{ISC}} - \frac{N_{T1}}{\tau_{Phos}} \\
\frac{dN_{Tn}}{dt} &= \frac{\sigma_{T1n}N_{T1}I}{\hbar\omega} - \frac{N_{Tn}}{\tau_{Tn1}},
\end{aligned} \tag{9}$$

where I is the irradiance, z is the sample thickness, σ_{Sij} and σ_{Tij} are the singlet and triplet cross sections from their respective ground and excited states, τ_{Sn1} and τ_{Tn1} are the nonradiative relaxation lifetimes from upper excited states S_n and T_n, and τ_F and τ_{Phos} are decay lifetimes from S_1 and T_1 to the singlet ground state S_0.

1.2.3 Excited State Absorption via Two-Photon Absorption

It is necessary to pay special attention to the role of ESA in 2PA measurements. ESA induced by 2PA in an organic system was first observed and explained in 1974 by Kleinschmidt et al [43]. Without separating ESA from 2PA, $\delta_{2PA}(\omega)$ measured by nanosecond pulses could be incorrectly interpreted as being two orders of magnitude larger than that obtained by femtosecond pulses [44]. In order to characterize 2PA induced ESA, pulsewidth dependent measurements are used in order to distinguish irradiance/fluence processes [45, 46]. ESA induced by 2PA, as shown in Fig. 2b, can be properly modeled by incorporating the 2PA term into the propagation and rate equations as [46, 47]:

$$\begin{aligned}
&\frac{\mathrm{d}I}{\mathrm{d}z} - \frac{\delta_{2PA} N_0 I^2}{\hbar\omega} - \sigma_{S1n} N_1 I \\
&\frac{\mathrm{d}N_0}{\mathrm{d}t} = -\frac{\delta_{2PA} N_0 I^2}{2(\hbar\omega)^2} + \frac{N_1}{\tau_F} \\
&\frac{\mathrm{d}N_1}{\mathrm{d}t} = \frac{\delta_{2PA} N_0 I^2}{2(\hbar\omega)^2} - \frac{N_1}{\tau_F} - \frac{\sigma_{S1n} N_1 I}{\hbar\omega} + \frac{N_n}{\tau_{Sn1}} \\
&\frac{\mathrm{d}N_n}{\mathrm{d}t} = \frac{\sigma_{S1n} N_1 I}{\hbar\omega} - \frac{N_n}{\tau_{Sn1}}.
\end{aligned} \tag{10}$$

1.3 Linear π-Conjugated Molecular Systems

Cyanine and cyanine-like dyes have been known for more than a century and have found numerous applications as photosensitizers in photography and photodynamic therapy, fluorescent probes in chemistry and biology, active and passive laser media, materials for nonlinear optics and electroluminescence, memory devices etc. [48, 49]. They are among a particular class of organic compounds that exhibit large (with molar absorbance up to 3×10^5 M^{-1} cm^{-1}) and tunable absorption bands in the visible and NIR regions, which is important for the development of organic materials with large third-order nonlinearities for all-optical signal processing [50]. Based on the number of methine (−CH=) groups in the π-conjugation, linear conjugated dyes can be divided into two categories: *polymethine* and *polyene dyes*. *Polymethines* are compounds made up from an *odd number* of methine groups bound together by alternating single and double bonds, which form a π-conjugated chain bridging together two terminal groups R_1 and R_2 as shown in Fig. 3a.

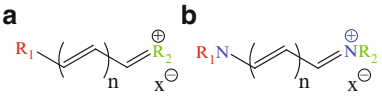

Fig. 3 (**a**) Typical *polymethine* and (**b**) *cyanine* molecular structures; *n* is the number of methine groups and X are counter ions

Polyenes are compounds made up from an *even number* of methine groups (not shown). These two classes of structures have different charge distribution and bond length alternation (BLA) along the main conjugation chain, thus leading to different electronic state configurations. Polymethine dyes are characterized by equalization of bond lengths and large charge alternation between neighboring carbon–carbon atoms in the π-conjugated chain. In contrast, polyene dyes have large BLA, while maintaining similar charges along the conjugated chain [51]. These two types of dyes typically have distinctive electronic structures, and thus differ by their linear and nonlinear optical properties. The influence of BLA to nonlinear optical properties is described in [52]. Simplified polymethine and cyanine dye structures are shown in Fig. 3. *Cyanine dyes*, which belong to the polymethine family, consist of *nitrogen atoms* at the end of the conjugated chain as shown in Fig 3b.

The electronic properties of these dyes can be tailored by changing the length of conjugation chain or by adding specific terminal groups R_1 and R_2. Due to their different electron affinities, these terminal groups can be classified into electron acceptor (A), and electron donor (D) groups.

Appending different terminal groups to the π-conjugated ends, the cyanine-like molecules may have the following molecular structures: D–π–D, D–π–A, and A–π–A. Additionally, electron acceptor/donor groups may be included into the main π-conjugation chain to form D–π–A–π–D or A–π–D–π–A quadrupolar structures. These basic structures are shown schematically in Fig. 4 and discussed in detail in Sect. 3.

Previously, 2PA properties of π-conjugated chromophores have been investigated primarily for molecules with absorption bands in the visible range (400–650 nm) [1, 15]. NIR cyanine-like dyes are now being developed due to their large optical nonlinearities, which makes them potentially applicable for fluorescence imaging, optical power regulation in the telecommunication wavelength range [53], and for all-optical signal processing [54]. A detailed analysis of the linear and nonlinear optical properties of the various symmetrical and asymmetrical cyanine and cyanine-like dyes will be discussed in Sect. 4.3. Throughout the text, we use the labeling for polymethine dyes as PD or PDs, squaraine dyes as SD or SDs, and tetraone dyes as TD or TDs.

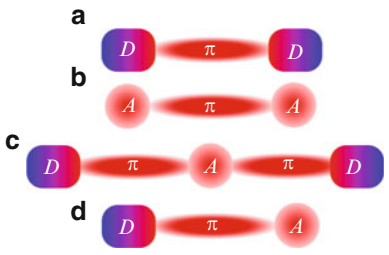

Fig. 4 Schematic of symmetrical (**a**) D–π–D, (**b**) A–π–A, (**c**) D–π–A–π–D, and (**d**) asymmetrical D–π–A molecular structures

2 Experimental Methodologies for Linear and Nonlinear Optical Characterization

To design organic conjugated molecules with optimal nonlinear optical properties, accurate and complete experimental analysis of their linear and nonlinear optical properties are needed. It is common to find in the literature reports of large nonlinear responses in different organic molecules; unfortunately, it is also not uncommon to encounter promising results due to erroneous or incomplete experimental analysis [55]. In the following section, we discuss different experimental techniques used for the nonlinear optical characterization of organic molecules.

Before being able to study the nonlinear optical properties of any material, it is necessary to have a complete understanding of its linear optical properties. Therefore, we start this section with a brief discussion of the techniques used to measure some of the most important linear properties, e.g., *linear absorption, fluorescence, anisotropy, and fluorescence quantum yield*.

2.1 Linear Optical Characterization

Two of the most important properties of any optical material are the linear absorption (one-photon) spectra and one-photon-excited fluorescence (1PF) spectra. In general, linear absorption spectra should be checked before and after each experiment to verify that the sample has not decomposed, especially after nonlinear optical measurement where photo-induced damage is often observed. All optical measurements, linear and nonlinear, should be performed at concentrations below the aggregation threshold, significant time should be given for the solute to fully dissolve, and the use of solution filters (filtration ~200 nm) can be useful for removing large aggregates. The ratio between the number of emitted photons and absorbed photons is known as the fluorescence quantum yield, Φ_F, and is an important parameter for all fluorophores.

In most cases, the *linear absorption* is measured with standard spectrometers, and the fluorescence properties are obtained with commercially available spectrofluorometers using reference samples with well-known Φ_F for calibration of the *fluorescence quantum yield*. In the ultraviolet and visible range, there are many well-known fluorescence quantum yield standards. Anthracene in ethanol ($\Phi_F = 0.27$) [56], POPOP in cyclohexane ($\Phi_F = 0.97$), Rhodamine 6G in ethanol ($\Phi_F = 0.95$), and Cresyl Violet in methanol ($\Phi_F = 0.54$) are among the most commonly used reference samples for wavelengths of 350–650 nm. For wavelengths longer than 650 nm, there is a lack of fluorescence references. Recently, a photochemically stable, D–π–D polymethine molecule has been proposed as a fluorescence standard near 800 nm [57]. This molecule, PD 2631 (chemical structure shown in Fig. 5) in ethanol, has $\Phi_F = 0.11$ and has its fluorescence peak at 809 nm. Fig. 5 compares the linear absorption and fluorescence spectra of the reference PD 2631 in ethanol to

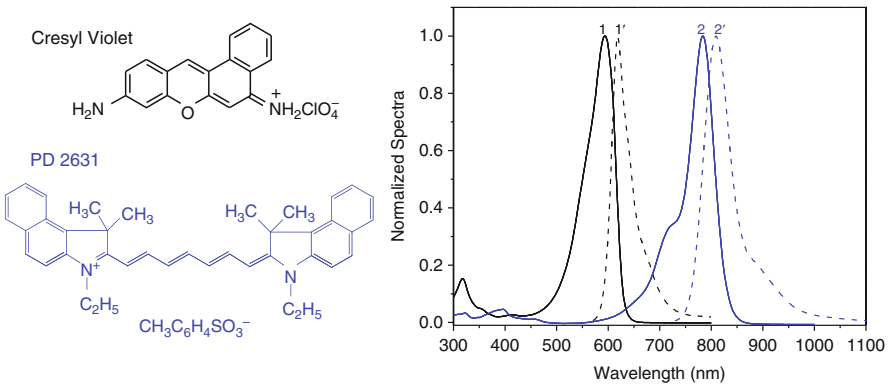

Fig. 5 Linear absorption (1, 2) and one-photon-excited fluorescence (1′, 2′) for the quantum yield standard Cresyl Violet (1, 1′) and the proposed standard PD 2631 (2, 2′) for NIR wavelengths. Molecular structures are shown to the *left*

the well-known standard Cresyl Violet in methanol. Additionally, a series of A–π–A dyes have been synthesized and show significant potential for fluorescence applications [58, 59]. The three shortest dyes (G37, G38, and G74) in Fig. 20 of Sect. 3.2.3 show good photochemical stability and surprisingly large one-photon fluorescence quantum yields of ∼0.90, ∼0.66, and ∼0.18 at the red to NIR region of ∼640 nm, ∼730 nm, and ∼840 nm, respectively.

Another important linear parameter is the *excitation anisotropy* function, which is used to determine the spectral positions of the optical transitions and the relative orientation of the transition dipole moments. These measurements can be provided in most commercially available spectrofluorometers and require the use of viscous solvents and low concentrations (c_M ∼1 μM) to avoid depolarization of the fluorescence due to molecular reorientations and reabsorption. The anisotropy value for a given excitation wavelength λ can be calculated as

$$r(\lambda) = \frac{I_{||}(\lambda) - I_{\perp}(\lambda)}{I_{||}(\lambda) + 2I_{\perp}(\lambda)}, \tag{11}$$

where $I_{||}(\lambda)$ and $I_{\perp}(\lambda)$ are the intensities of the fluorescence signal (typically measured near the fluorescence maximum) polarized parallel and perpendicular to the excitation light, respectively [41].

The anisotropy value $r(\lambda)$ ranges between −0.2 and 0.4 in correspondence with the angle γ between the absorption and fluorescence dipole moments, which can range from 90° to 0° in accordance to:

$$r(\lambda) = \frac{2}{5}\left(\frac{3\cos^2(\gamma) - 1}{2}\right). \tag{12}$$

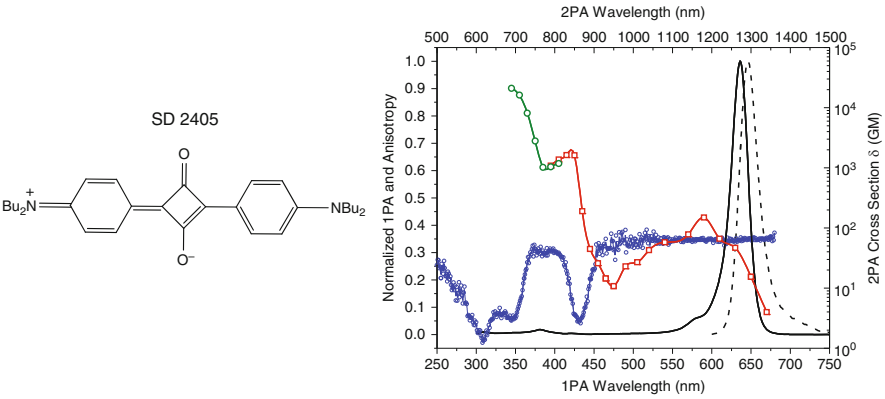

Fig. 6 Normalized linear absorption (*solid black line*), anisotropy (*blue circles*), and corresponding 2PA spectrum measured by two-photon fluorescence (*red squares*) and Z-scan (*green circles*) for SD 2405. Molecular structure is shown to the *left*

As seen from (12) and Fig. 6, the peaks in the excitation anisotropy spectrum indicate a small angle between the absorption and emission transition dipoles suggesting allowed 1PA transitions; while valleys indicate large angles between these two dipoles, suggesting a forbidden 1PA transition. Due to selection rules for symmetrical cyanine-like dyes, the valleys in the anisotropy spectrum could indicate an allowed 2PA transition as demonstrated in Fig. 6. Thus, an excitation anisotropy spectrum can serve as a useful guide to suggest the positions of the final states in the 2PA spectra.

From spectroscopic measurements, we can estimate the *fluorescence lifetime*, $\tau_F = \Phi_F \tau_N$, where the natural lifetime, τ_N, can be calculated from the Strickler–Berg equation in CGS units [60]:

$$\frac{1}{\tau_N} = 2.88 \times 10^{-9} n^2 \varepsilon^{\max} \left[\frac{\int F(\nu) d\nu \times \int \frac{\varepsilon(\nu)}{\nu} d\nu}{\int \frac{F(\nu)}{\nu^3} d\nu}, \right. \tag{13}$$

where $F(\nu)$ and $\varepsilon(\nu)$ are the normalized fluorescence and absorption spectra and $\varepsilon^{\max}$ (M^{-1} cm^{-1}) is the molar absorbance at the peak of the absorption band, and n is the refractive index of the solvent. For many cyanine-like molecules with spectral mirror symmetry between absorption and fluorescence spectra and small changes in excited state geometry, (14) gives reasonably good agreement with directly measured lifetimes. Thus, linear spectroscopic measurements allow the calculation of the values for the *transition dipole moments*, μ_{01}, an important parameter for 2PA, in CGS units as:

$$\mu_{01} = \sqrt{\frac{1,500(\hbar c)^2 \ln(10)}{\pi N_A E_{01}} \int \varepsilon_{01}(\nu) d\nu}, \tag{14}$$

where $\varepsilon_{01}(v)$ is the molar absorbance, N_A is Avogadro's number, and E_{01} is the energy at the absorption peak [41]. Calculations indicate that all cyanine-like dyes have similar μ_{01} values ranging from 10 to 17 D.

Summarizing, the linear optical characterization not only reveals important properties of organic molecules but also provides a necessary background for the nonlinear optical characterization, which will be discussed in the next section.

2.2 Nonlinear Optical Characterization

The term nonlinear optical property refers to an optical property, which can be modified by exposing the material to intense light irradiation. In this section, we focus on the cascaded first- ($\chi^{(1)}$) and third-order ($\chi^{(3)}$) susceptibilities describing nonlinear absorption (ESA and 2PA) and nonlinear refraction (n_2) processes. Z-scan, pump-probe, and two-photon upconverted fluorescence techniques are among the most used experimental methods for determining optical nonlinearities.

2.2.1 Pump-Probe Technique

The *pump-probe technique* is a method that can be used for determining lifetimes of excited states and their anisotropy. This method is the most common technique for time-resolved studies. A strong laser pulse (pump) is used to change the optical properties of the sample and a much weaker pulse (probe, with irradiance usually less than 10% of the pump irradiance) is used to study the magnitude and time evolution of the induced changes. The time evolution is investigated by delaying the probe pulse with respect to the pump. In this way, the pump-probe method can be applied to measure many nonlinear optical mechanisms, like nondegenerate 2PA and ESA. The temporal accuracy of the measurements is defined mainly by the pulse width of the laser beam used.

For 2PA measurements using the pump-probe technique, it is preferable to use femtosecond excitation due to the large irradiance to energy ratio. However, for ESA studies, both picosecond and femtosecond excitation can be used, since for most organic molecules the ESA lifetime is on the order of picoseconds to nanoseconds. The ESA spectrum can easily be obtained by the pump-probe technique, pumping the sample at the peak linear absorption (or slightly blue shifted from the main transition) and probing at a wavelength where ESA is expected, typically at shorter wavelengths compared to the pump, but longer probe wavelengths can give information about other, typically less intensive, ESA transitions. Currently, it is common to use a femtosecond white-light continuum, WLC, as the probe to obtain a spectrum. These can be generated in wide-bandgap crystalline materials, like CaF_2 or Sapphire, due to the broad WLC produced. In principle, a complete ESA spectrum can be obtained in a single laser shot experiment [61].

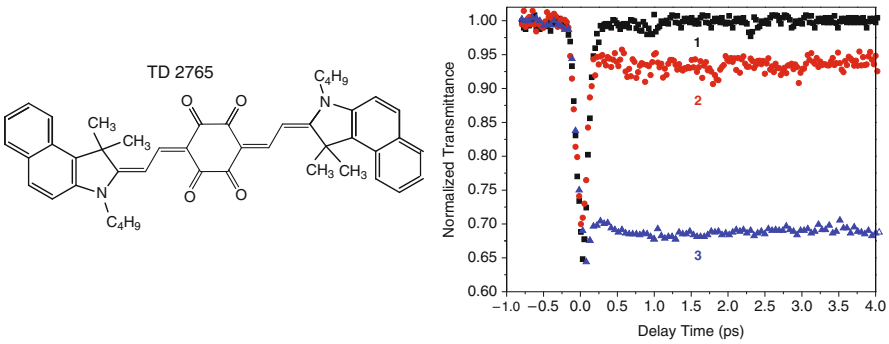

Fig. 7 Femtosecond pump-probe data for TD 2765 (molecular structure shown *left*). The probe wavelength is set at 670 nm and the pump wavelengths are (1) 710 nm, (2) 700 nm, and (3) 690 nm. See [62] for additional details

As discussed in Sect. 1.2.3, it is usually not possible to distinguish ESA from 2PA with Z-scan experiments if they are performed with only one excitation pulsewidth. However, since ESA is not an instantaneous process as is 2PA, the pump-probe technique can be successfully used to verify the origin of the nonlinearity for the spectral regions close to the main absorption band. Figure 7 illustrates how the influence of the ESA can be distinguished from the 2PA with pump-probe experiments. The curve labeled (1) shows an instantaneous 2PA response without ESA and the long-lived components of the transmittance change seen in (2) and (3) are due to ESA.

The pump-probe method can be also applied to measure the population decays or fluorescence lifetimes. For fluorescence lifetimes shorter than 100 ps, the relative polarization between pump and probe beams does not typically interfere with the decays. However, for longer lived excited states, the reorientation of the molecule, which typically takes hundreds of picoseconds, can play an essential role in decay kinetics and can affect the pump-probe results. When the reorientation time of the molecule is shorter or comparable to the fluorescence lifetime, the relative polarization of the pump and probe beams is important and the reorientation time has to be taken into account during the data analysis. To be able to eliminate the influence of the molecular reorientation on the pump-probe results, the angle between the pump and probe polarization is fixed at 54.7°, which is known as the "magic angle" (the 3-D analogy of 45 degrees) [63], which represents the angle at which the effects of the reorientation of the molecules cancel each other. Polarization-resolved pump-probe data can be fit using:

$$\begin{aligned} \Delta T_{||}(t) &= \Delta T_{\text{magic}}(0)\exp(-t/\tau_{\text{F}})[1+2r(0)\exp(-t/\tau_{\text{Rot}})] \\ \Delta T_{\text{magic}}(t) &= \Delta T_{\text{magic}}(0)\exp(-t/\tau_{\text{F}}) \\ \Delta T_{\perp}(t) &= \Delta T_{\text{magic}}(0)\exp(-t/\tau_{\text{F}})[1-r(0)\exp(-t/\tau_{\text{Rot}})], \end{aligned} \tag{15}$$

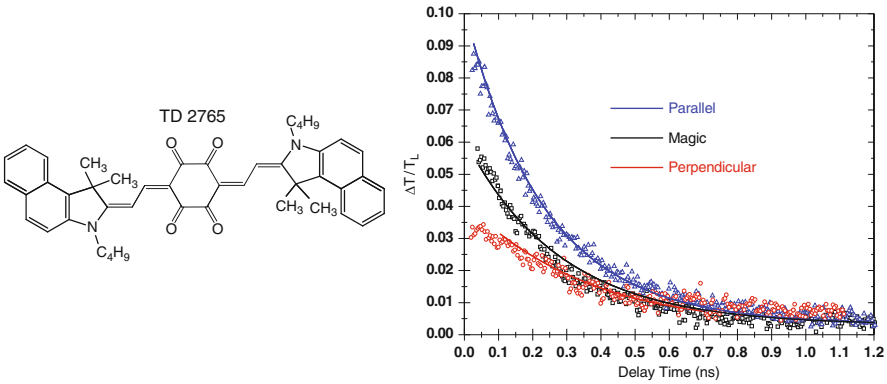

Fig. 8 Polarization-resolved picosecond pump-probe data for TD 2765 in ethanol (molecular structure shown *left*). The orientations of the probe beam relative to the pump are: perpendicular (*red*), "magic angle" (*black*), and parallel (*blue*). Data is modeled using (15) to obtain $\tau_F = 280$ ps, $\tau_{Rot} = 550$ ps, and $r = 0.35$. See [62] for additional details

where $\Delta T_{||}(t)$, $\Delta T_{\text{magic}}(t)$, and $\Delta T_{\perp}(t)$ are the change in transmittance measured for parallel, magic, and perpendicular probe polarizations with respect to the pump polarization, respectively, τ_F and τ_{Rot} are the fluorescence lifetime and molecular rotational lifetime, and $r(0)$ is the anisotropy at $t = 0$. Figure 8 and (15) show how molecular reorientation can influence the pump-probe results. If the magic angle is not used in the experimental setup, an over- or underestimation of the decay lifetime, τ_F, will be obtained for parallel and perpendicular polarizations respectively.

2.2.2 Z-Scan Technique

The *Z-scan technique*, first introduced in 1989 [64, 65], is a sensitive single-beam technique to determine the nonlinear absorption and nonlinear refraction of materials independently from their fluorescence properties. The simplicity of separating the real and imaginary parts of the nonlinearity, corresponding to nonlinear refraction and absorption processes, makes the Z-scan the most widely used technique to measure these nonlinear properties; however, it does not automatically differentiate the physical processes leading to the nonlinear responses.

The Z-scan technique is performed by scanning the sample through the focus of a Gaussian beam (the technique can be performed with any beam shape, but in practice, modeling of a Gaussian beam is preferred). The transmission through the sample is measured as a function of the Z position (with respect to the focal point $Z = 0$) and, consequently, of the beam waist. The change in transmission as a function of the beam waist (which corresponds to a function of fluence and/or irradiance) gives information pertaining to the nonlinear absorption (so-called

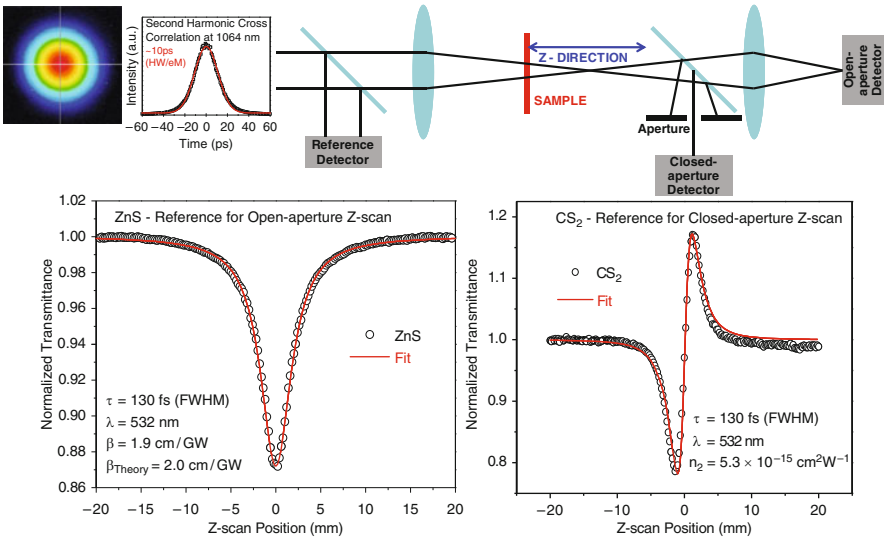

Fig. 9 Schematic of simplified Z-scan setup, and examples of open- and closed-aperture measurements of the common reference materials zinc sulfide (ZnS) and carbon disulfide (CS_2) with fitting using the theory proposed by [66]

open-aperture Z-scan). Adding an aperture after the sample, before any focusing element and linearly transmitting ~30% [66], the nonlinear phase change can be detected by changes in transmittance through the aperture onto the detector. When the nonlinear absorbance has been taken into account, this corresponds to the nonlinear refraction. Figure 9 demonstrates a simplified Z-scan setup together with examples of both the open- and closed-aperture experiments and their fitting using the theory proposed by Sheik-Bahae et.al. [66]. The fitting is done assuming a perfectly Gaussian laser beam and applying the "thin sample" approximation [66]. Knowledge of the beam, both spatially, by use of beam profiling cameras and knife-edge scans [67, 68] to determine focused spot sizes and propagation constants, and temporally, by use of fast detectors and autocorrelation techniques [69, 70], are needed to accurately analyze results.

For 2PA or ESA spectral measurements, it is necessary to use tunable laser sources where optical parametric oscillators/amplifiers (OPOs/OPAs) are extensively used for nonlinear optical measurements. An alternative approach, which overcomes the need of expensive and misalignment prone OPO/OPA sources, is the use of an intense femtosecond white-light continuum (WLC) for Z-scan measurements [71, 72]. Balu et al. have developed the WLC Z-scan technique by generating a strong WLC in krypton gas, allowing for a rapid characterization of the nonlinear absorption and refraction spectra in the range of 400–800 nm [72].

The main advantage of the usual Z-scan technique is that this method allows for a direct measurement of the nonlinearity, not requiring the use of reference samples, and thus minimizing experimental errors. On the other hand, the necessity of

having a fully characterized (spatially and temporally) Gaussian laser beams requires perfect alignment at each wavelength, making spectral determination time consuming. The WLC Z-scan is a promising technique to reduce the time needed to obtain spectra using the traditional Z-scan. From the open-aperture Z-scan trace, and the dependence of the signal on the energy per pulse, it is possible to verify the order of the nonlinear absorption process involved in the measurement. Note that in the spectral regions where there is linear absorption, 1PA followed by ESA (an RSA mechanism) can be confused with 2PA since both processes involve two photons. In this case, single pulsewidth Z-scan measurements cannot determine which physical process is occurring. However, one can separate these two processes by performing Z-scans with different pulse widths (ESA is fluence dependent while 2PA is irradiance dependent), or using time-resolved experiments such as pump-probe, which was discussed in Sect. 2.2.1.

For 2PA spectra measurements, it is preferable to perform Z-scans with femtosecond excitation due to the large laser irradiance with relatively low pulse energy. On the other hand, for ESA characterization, picosecond lasers are typically used due to their larger energy per pulse while maintaining an impulse excitation (as opposed to a nanosecond laser where the temporal pulse width is comparable to the excited state lifetimes). For this regime, picosecond Z-scans can be taken at different pulse energies (for example, 5 energies spanning at least one order of magnitude), and the ESA cross section can be calculated by simplifying the propagation and rate equations in (9) to only include singlet transitions (decay to the triplet states normally takes nanoseconds, but can be as short as picoseconds [42]). From these equations, a 3-level singlet model can be used assuming that the fluorescence lifetime is known (measured by pump-probe, or time-resolved fluorescence) and higher excited state lifetimes are much shorter than the excitation pulse width. For larger pump fluences, where the population of S_2 becomes significant, a fourth singlet level may need to be added to describe the complete process.

Shown in Fig. 10 are examples of fitting Z-scan results for a squaraine molecule where triplet states are significantly populated during picosecond excitation. In this case, femtosecond excitation was needed to determine the singlet parameters, shown in Fig. 10a. Picosecond excitation was required to model the full five-level system, shown in Fig. 10b [73], to determine the triplet parameters. To account for the triplet states, it is necessary to consider at a minimum the 5-level system shown Fig. 2 (three singlet and two triplet states). Typically, PDs do not populate triplet states during picosecond excitation [74, 75].

2.2.3 Two-Photon Fluorescence (2PF) Technique

The *2PF technique* measures the upconverted fluorescence induced by 2PA. This technique allows for the measurement of 2PA cross sections that are less than tens of GMs when the fluorescence quantum yield is large. The technique was first proposed by Kaiser et al. [76] in 1961 and represents an indirect way to measure the 2PA cross section, which can be calculated by comparing the integrated fluorescence signal

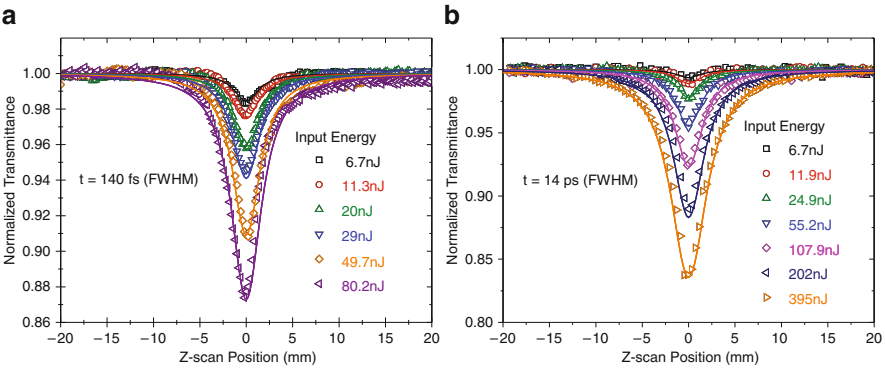

Fig. 10 Example of fitting Z-scan data for a squaraine molecule for (**a**) a 3-level model (singlet states only) with femtosecond excitation and (**b**) a 5-level model (both singlet and triplet states) with picoseconds excitation. The schematic is shown in Fig. 2a and the propagation and rate (9) are used for modeling

from an unknown molecule to a reference molecule with known 2PA cross section measured under identical conditions. The most common reference molecules are Rhodamine B in Methanol and Fluorescein in H_2O (pH = 11) [77]. Assuming that one knows the fluorescence quantum yields, Φ_F, (calculated as described in Sect. 2.1) and the concentrations, c_M, of the sample and reference and the 2PA cross section for the reference, Φ_{FRef}, the 2PA cross section for the sample can be calculated from:

$$\delta_{2PAsample} = \frac{\langle F\rangle_{sample}\Phi_{Fref}\, c_{Mref}\langle P\rangle_{ref}^2}{\langle F\rangle_{ref}\Phi_{Fsample}\, c_{Msample}\langle P\rangle_{sample}^2}\,\delta_{2PAref} \tag{16}$$

where $\langle F\rangle$ is the integrated fluorescence and $\langle P\rangle$ is the average pump power.

The experiment is performed with a spectrofluorometer similar to the ones used for linear fluorescence and quantum yield measurements (Sect. 2.1). The excitation, instead of a regular lamp, is done using femtosecond pulses, and the detector (usually a photomultiplier tube or an avalanche photodiode) must either have a very low dark current (usually true for UV–VIS detectors but not for the NIR), or to be gated at the laser repetition rate. Figure 11 shows a simplified schematic for the 2PF technique.

The 2PA cross section is a molecular parameter and, therefore, both techniques of Z-scan and 2PF should yield identical results when performed properly. From extensive investigations of many organic molecules, Z-scan and 2PF experiments complement each other, filling different spectral ranges and providing a double-check of the results. Figure 12 shows the 2PA spectrum measured for an extended dithiolene molecule [72], shown using open-aperture single-wavelength and WLC Z-scans, and the 2PF method. Figures 19, 23, and 24 also show excellent agreement between independently measured Z-scan and 2PF.

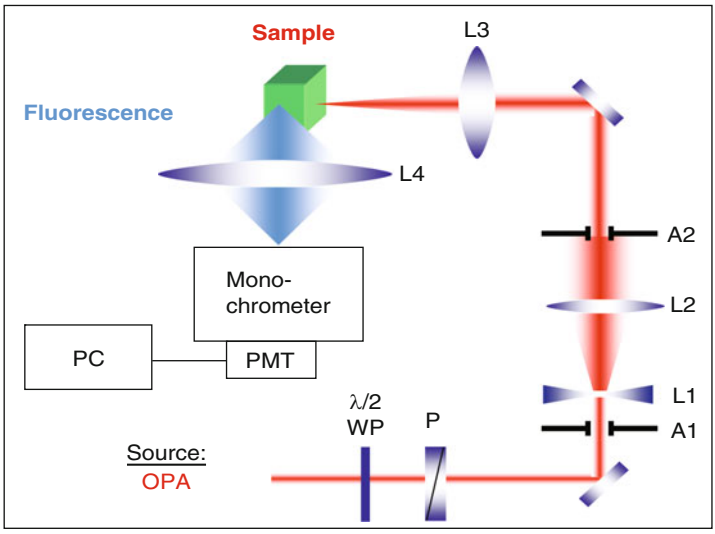

Fig. 11 Experimental setup for 2PF measurements. L are lenses, A are apertures, P is a polarizer, and WP is a half waveplate

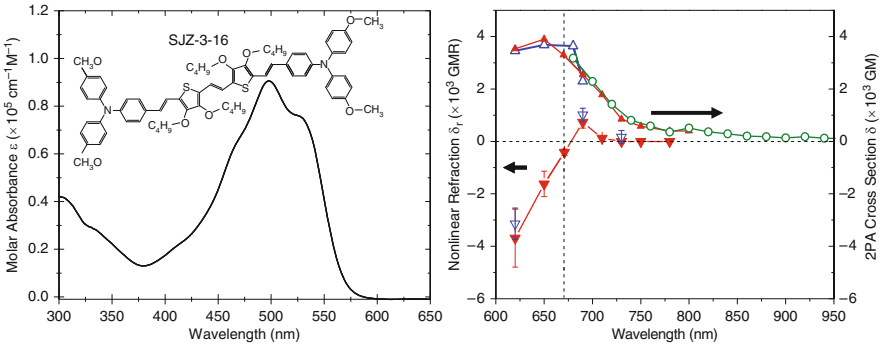

Fig. 12 (**a**) Molar absorbance and molecular structure (inset) for SJZ-3-16. (**b**) Comparison of the 2PA measured by single wavelength open-aperture Z-scan (*blue upward triangles*), WLC open-aperture Z-scan (*red upward triangles*), and 2PF (*green circles*). The nonlinear refraction measured by closed-aperture single wavelength (*blue downward triangles*), and WLC (*red downward*).

In conclusion, we stress that the complementary NLO characterization techniques of pump-probe, Z-scan, and 2PF allow for the unambiguous determination of nonlinear optical processes in organic materials. The important molecular parameters of 2PA cross section, fluorescence efficiency, reorientation lifetimes, excited state cross sections, etc. can be determined.

3 Trends in Dye Design and Structure–Property Relations

In order to design the best molecules for nonlinear optical applications, a link between molecular structure and two-photon absorption properties must be developed. To provide this link, one must start from an understanding of the formation of one-and two-photon absorption spectra in a series of molecules with systematic changes in structure. Detailed experimental characterization combined with quantum-chemical calculations and modeling can give the necessary information for the development of a design strategy. In this section, we show the connection between efficient 2PA and various elements of molecular structure, such as the length of the conjugated chromophore, the types of substitutions, including symmetrical and asymmetrical combinations of electron donor and acceptor terminal groups, and the addition of such groups in the middle of the chromophore.

3.1 Extending Absorption into the NIR

Before discussing the ways to enhance the 2PA cross section, we consider one of the most important and useful properties of cyanine-like dyes – the possibility to tune their absorption bands from the visible to NIR region up to ~1,600 nm. The shift of absorption spectra into the NIR region can be accomplished using two methods: lengthening the polymethine chromophore (polymethine chain) or by introducing specific terminal groups with their own extended conjugation system, which can strongly interact with the main chromophore and extend the total effective length of conjugation in the molecule [57, 78]. The first method typically decreases photochemical stability of the molecules, which can be partially improved by the introduction of bridge units within the chain. However, the second method allows significant shifting of the absorption bands without a substantial decrease of the photochemical stability. This method is described in [57] and is demonstrated in Fig. 13 for two sets of polymethine, squaraine, and tetraone dyes having similar lengths of the chain and different terminal groups.

The first set of dyes, so called "visible set", is presented by polymethine dye PD 2630, squaraine dye SD 2243, and tetraone dye TD 2765, all with benzo[*e*]indolium terminal groups. The second set of dyes, so called "NIR set", is presented by polymethine dye PD 2658, squaraine dye SD 2878, and tetraone dye TD 2824, all with 5-butyl-7,8-dihydrobenzo[*cd*]furo[2,3-*f*]indolium terminal groups. A distinguishing feature seen from this figure is a remarkably large, ≈300 nm, red shift of the absorption bands for PD 2658 and SD 2878 as compared to PD 2630 and SD 2243. The absorption spectrum of TD 2824 is red-shifted by ≈200 nm as compared to TD 2765. Thus, the effect of the 5-butyl-7,8-dihydrobenzo[*cd*]furo[2, 3-*f*]indolium terminal groups is equivalent to the extension of the chain to three vinylene groups.

Introduction of the acceptor squaraine and tetraone bridges to the conjugated chain causes BLA in the bridges resulting in a blue shift of the main absorption

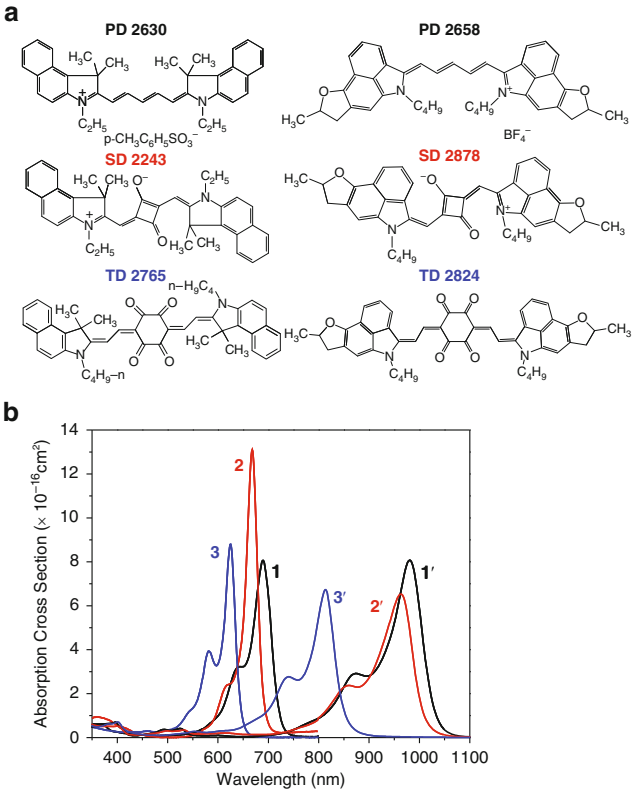

Fig. 13 (**a**) Molecular structures and (**b**) 1PA cross section of two sets of PDs, SDs, and TDs with similar chain lengths and different terminal groups. The first set of dyes (visible set) consists of PD 2630 (1), SD 2243 (2), and TD 2765 (3), all with benzoindolium terminal groups and the second (NIR set) is comprised of PD 2658 (1′), SD 2878 (2′), and TD 2824 (3′), all with benzofuroindolium terminal groups

bands. Additionally, incorporation of the stronger tetraone acceptor units leads to a larger BLA within the bridge and changes the nature of the molecules from polymethine to a polyenic type of conjugation with an even number of carbon atoms in the chain. Therefore, BLA for tetraone dyes are observed within the whole conjugated system, and their absorption spectra are more blue-shifted, especially for the NIR TD 2824 as compared to the corresponding PD 2658. The large red shifts for the "NIR set" of molecules can be explained by the extended π-system within the terminal groups and its strong conjugation with the π-system of the chain.

Linear absorption and fluorescence spectra for the series of symmetrical cationic polymethines with 5-butyl-7,8-dihydrobenzo[*cd*]furo[2,3-*f*]indolium terminal groups are shown in Fig. 14 for solvents of different polarity. It is known that the polarity of solvents can be characterized by their orientational polarizability, which is given by $\Delta f = (\varepsilon - 1)/(2\varepsilon + 1) - (n^2 - 1)/(2n^2 + 1)$, where ε is the static dielectric constant and n is the refractive index of the solvent [41]. Calculated Δf values

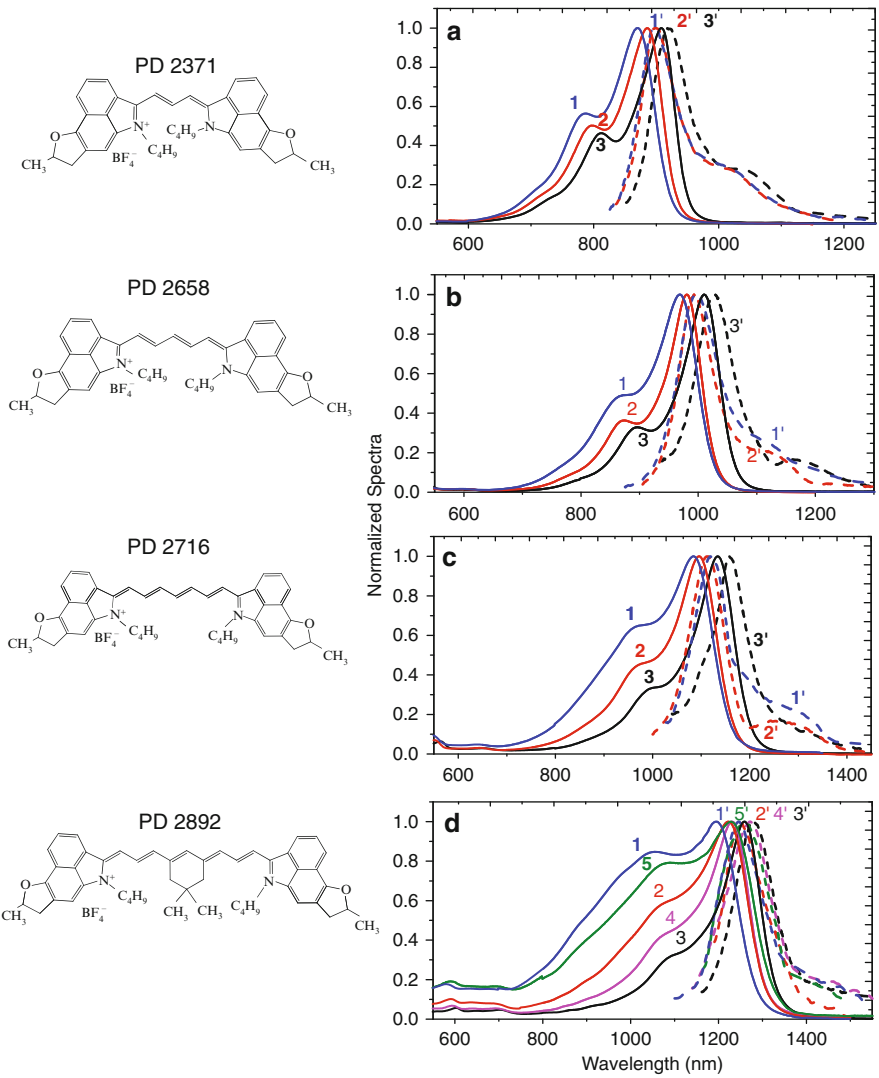

Fig. 14 (*left*) Molecular structures and (*right*) 1PA (*solid lines* 1, 2, 3, 4, 5) and 1PF spectra (*dashed lines* 1′, 2′, 3′, 4′, 5′) for PD 2371 (**a**), PD 2658 (**b**), PD 2716 (**c**), and PD 2892 (**d**) in acetonitrile (1, 1′), butanol (2, 2′), dichlorobenzene (3, 3′), methylene chloride (4, 4′), and dimethyl sulfoxide (5, 5′), respectively

range from the smallest polarity of 0.208 for dichlorobenzene (cationic dyes cannot be dissolved in solvents of lower polarity) to the largest in this series of 0.306 for acetonitrile (ACN).

The absorption spectra for all these dyes are composed of intense cyanine-like bands attributed to the $S_0 \rightarrow S_1$ absorption, with the main absorption peaks shifted by ≈100 nm to longer wavelengths upon lengthening of the main conjugation

chain, and weak linear absorption in the visible and UV region corresponding to absorption to higher excited states $S_0 \rightarrow S_n$. Relatively short wavelength absorbing PDs exhibit classic nonpolar solvatochromism, i.e., a red shift of the absorption peak with an increase in solvent polarity, which correlates with a decrease of the refractive index. This is consistent with a symmetrical ground and excited state charge distribution and small permanent dipole moments, 1–2 D, oriented perpendicular to the polymethine chromophore [41]. In contrast, absorption spectra of PDs absorbing in the range of ≈1,000 nm demonstrate a strong dependence on solvent polarity, see Fig. 14. An increase in solvent polarity leads to a substantial band broadening represented by the growth of the short wavelength shoulder. This is a strong indication of polar solvatochromism, which is typical for dyes that exhibit charge localization and a large ground state permanent dipole moment. This effect was investigated earlier theoretically [79, 80] and experimentally [81] and explained by a *symmetry breaking effect*, leading to the appearance of a ground state structural form with asymmetrical charge distribution and, as a result, with an asymmetrical bond-length alternation. Our explanation is based on the previously proposed theoretical concept of the formation of charge density waves (or solitonic waves) in the linear conjugated chromophores [82]. In the theoretical paper [80], we show that the minimum number of vinylene groups, *n,* in the conjugated chain necessary to break the symmetry of the simple streptocyanine molecule, is eight in the gas phase and six in nonpolar cyclohexane. As the symmetry breaks, an additional absorption band with large oscillator strength appears in the electronic spectrum. Charge localization is additionally stabilized by the solvent, which increases the energy barrier between symmetrical and asymmetrical forms and results in ground state symmetry broken geometries occurring at a shorter (than in the gas phase) length of the conjugated system. An additional absorption peak at the shorter wavelength region corresponds to a molecular geometry with charge localized at one of the molecular terminal groups that is additionally stabilized by the solvent. This finding demonstrates the possibility of coexistence of the two forms in polar solutions. Thus, our results suggest that a solvatochromic effect may be an important factor in absorption band broadening.

Quantum-chemical calculations show that the symmetry of molecular geometry is conserved for polymethines with 5-butyl-7,8-dihydrobenzo[*cd*]furo[2,3-*f*]indolium terminal groups at $n = 1$–3. However, for longer molecules, starting from $n = 4$, calculations show an inequality of the corresponding bond lengths in the chain. We note that, experimentally, a substantial broadening of the absorption band in polar ACN is observed even for tricarbocyanine PD 2716 ($n = 3$), as shown in Fig. 14. Therefore, we suggest that the existence of the asymmetrical form in the polar solvent may be observed in this series of polymethines starting from $n = 3$. An increase in solvent polarity shifts the equilibrium between these two forms to favor the asymmetrical form. Experiments show that the less polar solvent primarily stabilizes the symmetrical form.

In contrast to the absorption spectra, fluorescence spectra for all polymethine molecules are similarly narrow, independent of the solvent polarity, indicating that emission originates from the symmetrical form only. The symmetry breaking effect

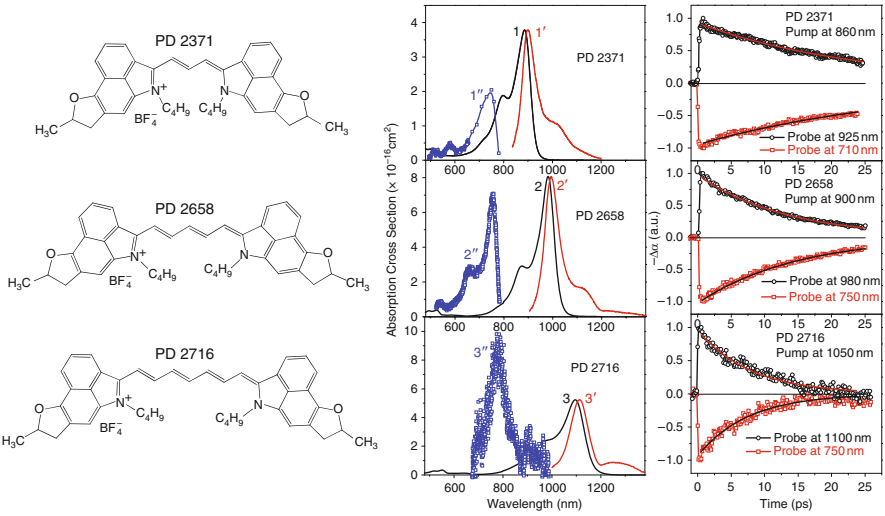

Fig. 15 (*left*) molecular structures; (*center*) 1PA (1, 2, 3), 1PF (1′, 2′, 3′), and ESA cross sections (1″, 2″, 3″) of PD 2371 (1, 1′, 1″), PD 2658 (2, 2′, 2″), and PD 2716 (3, 3′, 3″); (*right*) decay kinetics (Δα is the change of absorption of probe)

can also be responsible for the small quantum yields (typically less than 1%) and short lifetimes (typically less than 100 ps) for dyes absorbing in the range of ≈1,000 nm. We suggest that the most efficient route of energy deactivation is via formation of the asymmetrical excited state molecular geometry, which is strongly coupled to the ground state geometry.

The ESA spectra and decay kinetics of this series of polymethines are shown in Fig. 15. A small red shift of the ESA spectra (comparing to a large red shift of the 1PA main band) is observed as the conjugation length increases. Lengthening of the conjugation chain also leads to an increase of both the ESA cross section peak values and the ratio of the total ESA to total 1PA main transition bands, which are proportional to their oscillator strengths. These totals are defined as the integrated area in a plot of absorbance versus photon energy. For PD 2716 with $n = 3$, the oscillator strength for ESA can be as large as that of the ground state, which is favorable for some nonlinear optical applications [78]. To obtain the decay kinetics of the series of polymethines shown in Fig. 15, the samples are pumped at their 1PA peaks and probed first, near the 1PA peaks where saturable absorption occurs and second, in the region of reverse saturable absorption. Both saturable and reverse saturable absorption decays show the same lifetimes (corresponding to the lifetime of the S_1 state) for all polymethine dyes. This confirms that no other intermediate states are involved with the ESA process. The lifetime of the S_1 state, shown in the decay kinetics, decreases as the conjugation length increases, which is also in accord with the decrease of their fluorescence quantum yields [78].

From these studies, we find that the dyes with dihydrobenzo[cd]furo[2,3-f] indolium terminal groups are characterized by a remarkably large shift of their

linear absorption bands to the red region (300 nm for PDs and 200 nm for SDs). These large red shifts for the "NIR" set of molecules can be explained by the extended π-system within the terminal groups and their strong connection with the π-system of the chain resulting in a significant extension of the total effective conjugation length. The effect of these terminal groups is equivalent to the extension of the chain to three vinylene groups. This is specifically true for PDs with benzo[e]indolium terminal groups.

In the next sections, we systematically describe structure–property relations in symmetrical (Sect. 3.2) and asymmetrical (Sect. 3.3) series of cyanine-like molecules.

3.2 *Symmetrical π-Conjugated Cyanine-Like Systems*

3.2.1 Cationic D–π–D Dyes

Molecular structures of a series of cationic D–π–D dyes, and their 1PA and 2PA spectra are shown in Fig. 16. These dyes have increasing lengths of conjugation and share the same indolium terminal groups, which are electron donors. *An increase of conjugation length* by one unit leads to a red shift of the one-photon main absorption band by ∼100 nm [83]. 2PA spectra for all these D–π–D molecules show one weak band corresponding to two-photon excitations into the vibrational shoulder of the main $S_0 \rightarrow S_1$ absorption band, which is weakly allowed due to vibronic coupling; and a second much stronger band, corresponding to two-photon

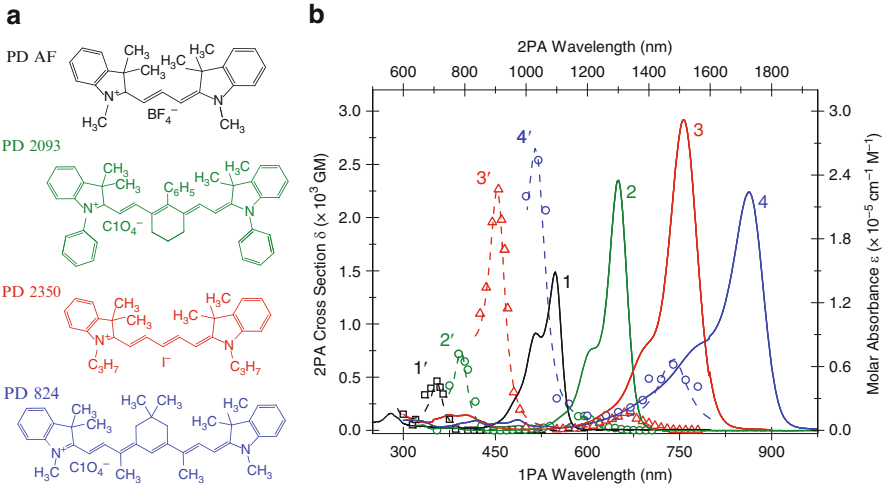

Fig. 16 (**a**) Molecular structures of PD AF ($n = 1$), PD 2093 ($n = 2$), PD 2350 ($n = 3$), and PD 824 ($n = 4$); (**b**) 1PA and 2PA bands for of PD AF (1, 1′), PD 2093 (2, 2′), PD 2350 (3, 3′), and PD 824 (4, 4′), respectively

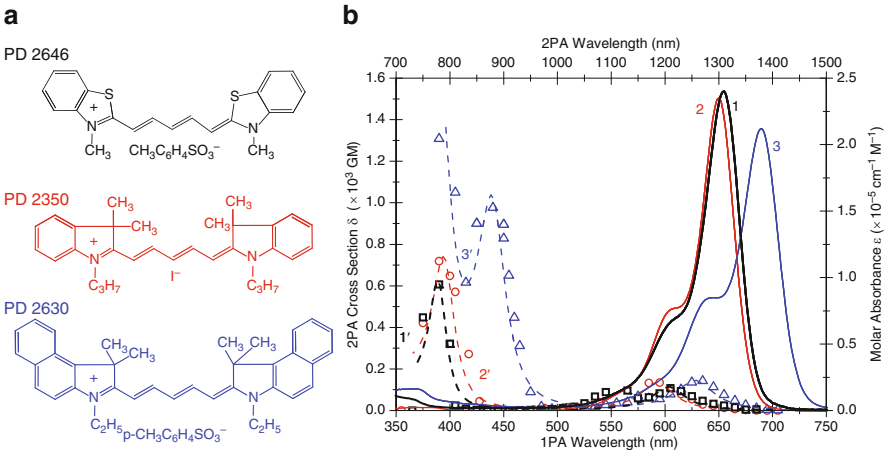

Fig. 17 (**a**) Molecular structures and (**b**) 1PA and 2PA of PD 2646 (1, 1′), PD 2350 (2, 2′), and PD 2630 (3, 3′), respectively

excitation into the S_2 state. In correspondence with (8), lengthening of the conjugation chain leads to increase in magnitude of 2PA cross sections. This can be explained by an increase of the ground state transition dipole moment and a decrease in detuning energy. Lengthening the chain results in an increase of δ_{2PA} for the first 2PA band from 10 to 600 GM and for the second 2PA band from 470 to 2,550 GM (see Fig. 16). However, it is worth noting that an increase of conjugation length could also lead to symmetry breaking for long wavelength absorbing dyes (seen for PD 824), resulting in an asymmetrical charge distribution within the conjugated chain [83], which affects 2PA cross sections.

To investigate the *effect of the donor properties* of the terminal groups, we compare a series of molecules with the same conjugation length ($n = 2$), but different terminal groups, see molecular structures in Fig. 17a. The electron donor strength increases from thiazolium (PD 2646), to indolium (PD 2350), and to benzoindolium (PD 2630) terminal groups. From Fig. 17b, it is clearly seen that an increase in the donor strength leads to an increase of the 2PA cross section. A more detailed description of structure–property trends in a series of cationic D–π–D dyes is presented in [83].

3.2.2 Neutral D–π–A–π–D Dyes

The addition of an electron acceptor group into the D–π–D can further enhance the 2PA cross sections. A series of dyes, cationic PD 2630, and two neutral dyes, SD 2243 and TD 2765, are shown in Fig. 18a. Compared with the polymethine dye PD 2630, SD 2243 has a squaraine fragment and a strong electron acceptor inserted into the main conjugation chain, while TD 2765 contains a tetraone fragment and an

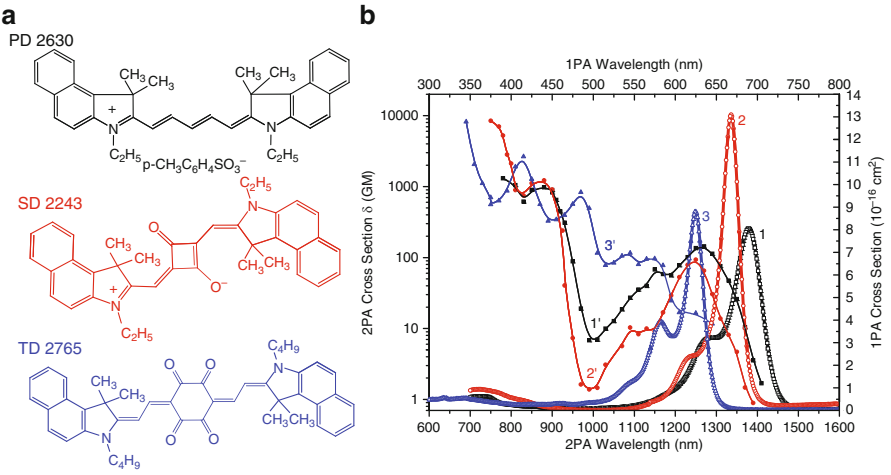

Fig. 18 (**a**) Molecular structures of PD 2630, SD 2243, TD 2765; (**b**) 1PA and 2PA of PD 2630 (1, 1′), SD 2243 (2, 2′), TD 2765 (3, 3′), respectively

even stronger electron acceptor group. As seen from Fig. 18b, the introduction of acceptors leads to a blue shift of the 1PA main transition band. The 2PA cross section of SD 2243 increases by ~6 times compared to PD 2630 at its 750 nm 2PA wavelength; while TD 2765 shows broader 2PA bands with a nearly monotonic increase of δ_{2PA} (ω) towards the 1PA edge. The difference of 2PA between D–π–A–π–D dyes and D–π–D dyes can be explained by the intermediate state resonance enhancement (ISRE) due to a narrowing of the 1PA main transition band, and by an increase in the density of final states, which is supported by quantum-chemical calculations.

A detailed experimental investigation and quantum-chemical analysis of 2PA spectra for quadrupolar D–π–A–π–D structures in cyanine-like molecules are presented in [62].

3.2.3 Anionic A–π–A Dyes

A series of anionic A–π–A dyes with different conjugated chains (G37, G38, G74, and G152) is obtained by connecting two diethylamino-coumarin-dioxaborine acceptors (A) via a π-conjugation (see Fig. 20a for molecular structures) [58]. The linear absorption, fluorescence, anisotropy, and 2PA spectra are shown in Fig. 19. 2PA spectra for all these A–π–A molecules show one weak band corresponding to two-photon excitations into the vibrational shoulder of the1PA main transition band and one or two much stronger bands, corresponding to two-photon excitations into S_2 and higher electronic states. Similarly to that for symmetrical cationic D–π–D dyes, an increase of conjugation length leads to both a red shift of the 2PA transition bands and an increase of δ_{2PA} (ω). The longest dye, G152, has a large δ_{2PA} (ω) of

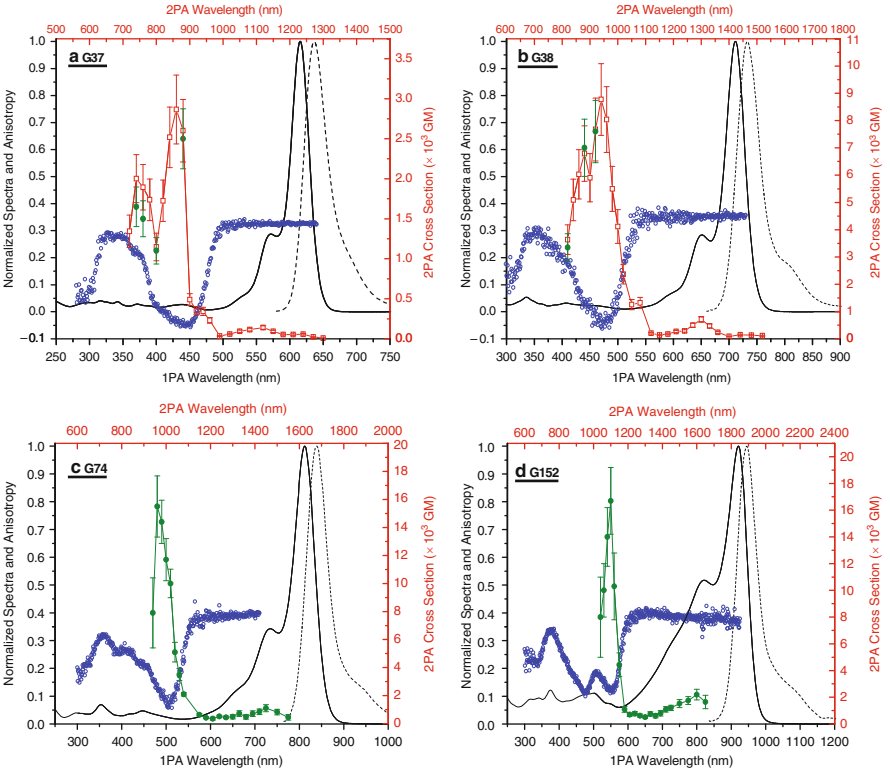

Fig. 19 1PA (*solid black lines*), 1PF (*dashed black lines*), anisotropy (*blue circles*), and 2PA spectra measured by 2PF (*red squares*) and Z-scan (*green circles*) of G37, G38, G74, and G152 in ACN. *Red axes* correspond to 2PA measurements

≈16,000 GM at its peak and a δ_{2PA} (ω) of ≈2,000 GM at 1,600 nm (near telecommunication wavelengths of 1,300–1,600 nm) which is one of the largest reported 2PA cross section for organic molecules in this wavelength range. These large 2PA cross sections are explained by the combination of very large transition dipole moments of μ_{01} ∼13–20 D and μ_{1F} ∼9–13 D, which is confirmed by quantum chemical calculations.

As seen from Fig. 19, fluorescence excitation anisotropy is a very useful tool to predict the positions of 2PA bands as was concluded in Sect. 2.1.

The ESA spectra of this series of A–π–A dyes are shown in Fig. 20. They exhibit broad and intense bands in the visible range (400–600 nm for G37, 400–630 nm for G38, 450–630 nm for G74, and 450–700 nm for G152) and weak bands in the NIR as revealed in Fig. 20 for G38. We observe that lengthening of the conjugation chain leads to a ≈30–40 nm red shift of the ESA peaks, which is similar to the behavior of D–π–D polymethine dyes. This red shift (∼30–40 nm) is much smaller than for the linear absorption bands (∼100 nm). Another experimental feature is connected with the redistribution of the ESA magnitude from the shorter to the

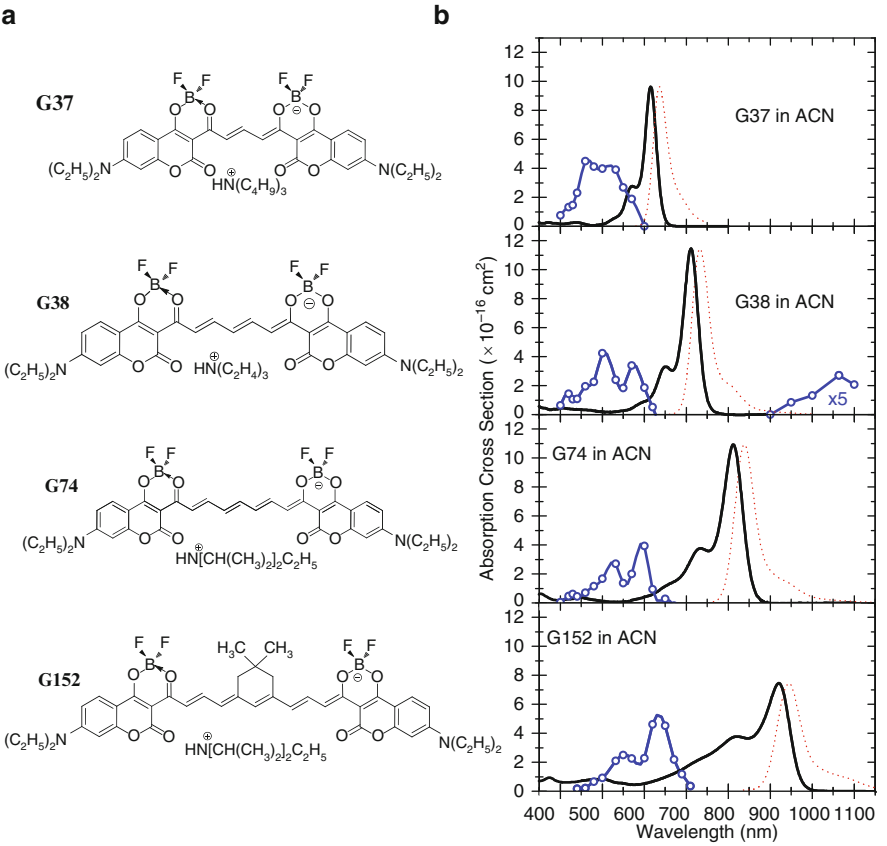

Fig. 20 (**a**) Molecular structures of G37 ($n = 1$), G38 ($n = 2$), G74 ($n = 3$), and G152 ($n = 4$). (**b**) 1PA (*solid black lines*), 1PF (*dashed black lines*), and ESA (*blue circles*) spectra

longer wavelength band. This redistribution is enhanced as the conjugation length increases and clearly observed for G152, which is probably a result of the involvement of a large number of excited state transitions.

A more detailed description of structure–property trends in a series of anionic A–π–A dyes is presented in [59].

3.3 *Asymmetrical π-Conjugated Cyanine-Like Systems*

The asymmetrical D–π–A dyes, often referred to as push–pull polyenes, are an additional class of cyanine-like molecules of interest. Due to their dipolar nature, the linear and nonlinear optical properties of this series of dyes can be strongly influenced by solvent polarity [84]. The structures of a series of such dyes (G19,

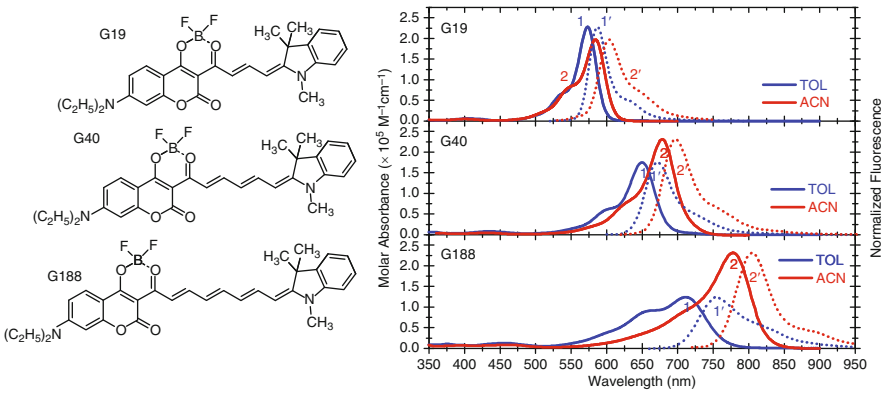

Fig. 21 (*left*) Molecular structures and (*right*) 1PA (1, 2) and 1PF (1′, 2′) spectra of G19, G40 and G188 in toluene (1, 1′) and ACN (2, 2′)

G40, and G188) with different conjugation lengths ($n = 1$–3) are shown in Fig. 21 with linear absorption and fluorescence spectra measured in two different solvents, toluene and ACN. All three dyes contain the same trimethylindolin donor group and diethylamino-coumarin-dioxaborine acceptor group. Significant solvent-dependent absorption and fluorescence spectra are observed for all three dyes. The main properties of these compounds can be explained based on the well-developed two-state model for push–pull polyenes as quasi-one-dimensional molecules containing an electron-donating group (D) and electron-accepting group (A) interacting via a π-conjugated chromophore [52, 85]. The structure of these molecules can be presented in two resonance forms: neutral D–π–A and ionic (or zwitterionic) with the separated charges D^+–π–A^-. Using this model in conjunction with extensive experimental data and quantum-chemical analysis, valuable insights may be gained for the explanation of the linear and nonlinear properties of G19, G40, and G188. Our understanding is that for the molecule G19 with the shortest conjugated chain, the donor–acceptor properties of the terminal groups in both solvents dominate the properties of the polyenic chain, and the ground state can be represented by a "polymethine-like" structure with almost equalized bond lengths within the conjugated chromophore and with the charges alternating at carbon atoms.

For the dye G188 with the longest conjugated chain, we suppose that the ground state represents a mixture of a "polymethine-like" structure, connected with the donor-acceptor properties of the terminal groups, and a "polyene-like" structure, mainly determined by a polyenic-type of conjugated chain with strong BLA. The relative contribution of these two resonance structures to the ground state is controlled by the polarity of the solvent: a more polar solvent can increase the ground state polarization and make the charge-separated form dominant. The neutral polyenic form dominates in less polar toluene resulting in a change of the absorption shape (growth of the short wavelength shoulder), clearly seen for G188 in Fig. 21. Dye G40 presumably represents an intermediate case between the shortest G19 and

the longest G188 based on linear absorption data and quantum-chemical analysis. Analyzing the shift of the absorption peaks with lengthening of the chromophore, we note that an increase in the conjugation length from G19 to G188 leads to a shift of ≈100 nm in ACN and ≈70 nm in toluene, which is in accord with the model presented of a co-existence of "polyenic-like" and "polymethine-like" forms. Asymmetrical D–π–A dyes show a bathochromic shift of the main absorption peaks, ≈11 nm for G19, ≈28 nm for G40, and ≈65 nm for G188, with increasing solvent polarity from toluene to ACN.

The solvatochromic behavior of these dyes in solution can be explained by the comparison of their permanent dipole moments. If the excited state exhibits a larger dipole moment (μ_1) than the ground state (μ_0), it is preferentially stabilized by the more polar solvent, and the energy between these two states decreases, that is, the absorption and emission spectra both shift to the red region.

Additionally, note that the polarity of the solvent significantly affects not only the positions of absorption and fluorescence spectra but also the fluorescence quantum yields. The largest difference in quantum yield is observed for G19 (eight times larger in toluene) [86]. The effect of solvent polarity on quantum yield and fluorescence lifetime was investigated in mixtures of toluene and ACN (polarity range 0.013–0.306). Polarity dependent quantum yield and lifetime measurements are presented in Fig. 22.

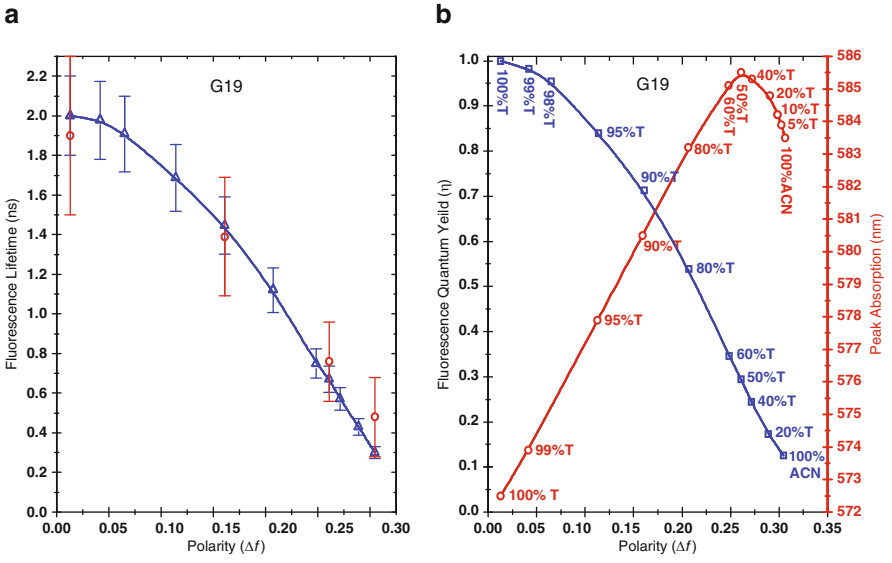

Fig. 22 (**a**) Comparison of fluorescence lifetime (*blue triangles*), calculated from (13), and measured by time-resolved fluorescence (*red circles*) as a function of solvent polarity for G19. (**b**) Fluorescence quantum yield (*blue squares*) and peak ground state absorption wavelength (*red circles*) as a function of solvent polarity given by the percentage of toluene (T) in toluene-ACN mixtures for G19

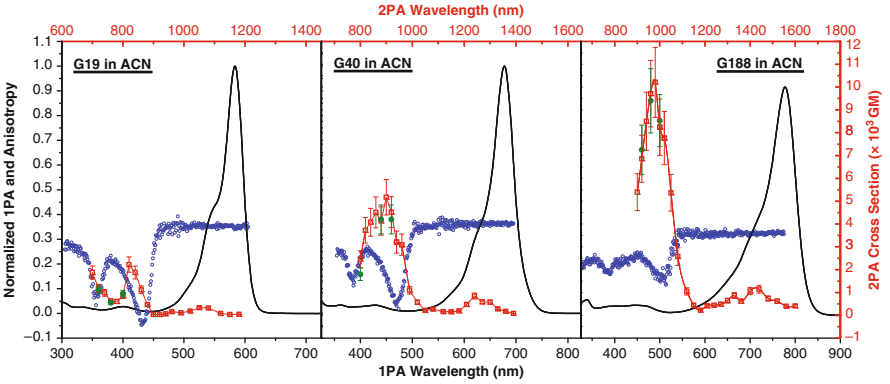

Fig. 23 1PA (*solid black lines*), anisotropy (*blue circles*), and 2PA spectra measured by 2PF (*red squares*) and Z-scan (*green circles*) of G19, G40, and G188 in ACN. *Red axes* correspond to 2PA measurements

It is seen that the fluorescence quantum yield and lifetime of G19 gradually decreases with increasing solvent polarity. For example, the insertion of 20% ACN by volume into toluene leads to a decrease of a factor of two. Based on these results we can conclude that G19 is very sensitive to solvent polarity and can be used as an efficient probe to test the polarity of its microenvironment. A reverse trend of the absorption peak at 1:1 mixture of ACN and toluene (50%T in Fig. 22b) corresponds to a change of the sign of μ_0–μ_1 due to a transition from a "polyene-like" structure in nonpolar toluene to a "polymethine-like" structure in polar ACN.

These spectroscopic studies have advanced our knowledge of the structure–property relations, which are extremely important for understanding the nonlinear optical behavior of these dyes, and specifically for their 2PA properties discussed below.

The 2PA spectra in ACN are shown in Fig. 23 in comparison to fluorescence excitation anisotropy. The increase of conjugation length leads to an increase of 2PA cross section as well as to a red shift of the peak the absorption. Interestingly, there is no significant indication of 2PA under the 1PA main peak, which is different from observation for typical asymmetrical dyes [86]. This is explained by quantum-chemical calculations due to the large angle between transition dipole moment μ_{01} and the change of permanent dipole moment, $\Delta\mu$, under excitation, see Sect. 1.2.1. The first weakly allowed 2PA band, similar to symmetrical dyes, can be attributed to the coupling between the first excited electronic state S_1 and its vibrational modes. The second, strongly allowed 2PA band is connected with two-photon excitation into S_2 and higher electronic states and corresponds approximately to the anisotropy valley as seen in Fig. 23. The peak of the third 2PA band for G19 could not be resolved due to the presence of 1PA edge.

In order to investigate the δ_{2PA} (ω) solvent dependence of the D–π–A dyes, the 2PA spectra of G188 in toluene and ACN are presented in Fig. 24. As large as two-fold enhancement of the second 2PA band is observed in ACN (10,000 GM)

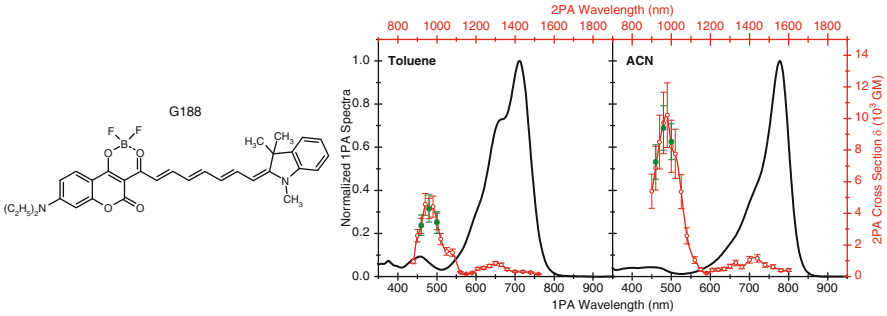

Fig. 24 1PA (*solid black lines*) and 2PA spectra measured by 2PF (*red squares*) and Z-scan (*green circles*) of G188 in ACN and toluene. *Red axes* correspond to 2PA measurements

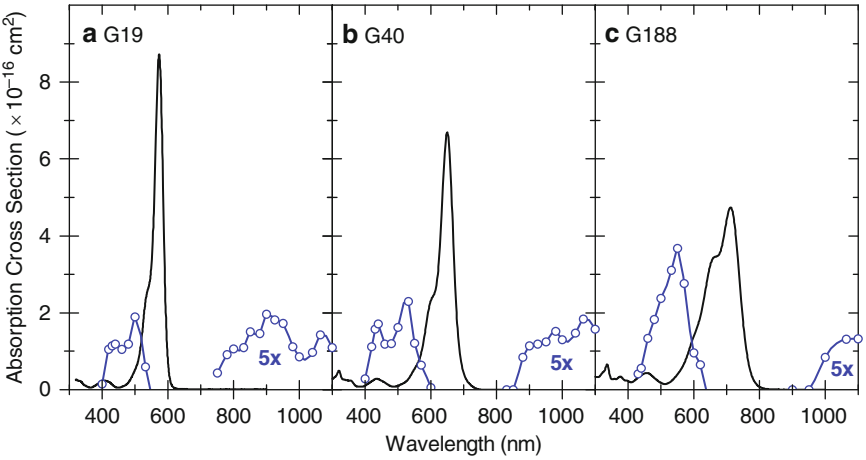

Fig. 25 1PA (*black*) and ESA (*blue*) of G19, G40, and G188 in toluene

comparing to toluene (4,600 GM), while the position of 2PA band does not shift in these two solvents. Since a large bathochromic effect is observed in the 1PA main transition band, this enhancement can be explained by ISRE due to the decrease of the energy difference between S_1 and S_0 in ACN [32, 86].

The ESA spectra of asymmetrical dyes in toluene are shown in Fig. 25. They show broad structureless bands in the NIR region (750–1,100 nm for G19, 850–1,100 nm for G40, and 950–1,100 nm for G188) and more intense transitions in the visible range (400–550 nm for G19, 400–600 nm for G40, and 450–650 nm for G188). Similarly to symmetrical anionic polymethine dyes (Fig. 20), the increase of conjugation length leads to a small red shift of ESA spectra, and to an enhancement of ESA cross sections and the ratio between the ESA and linear absorption oscillator strengths by approximately a factor of two. More detailed experimental description and quantum-chemical analysis can be found in [86].

3.4 Enhancement of 2PA Cross Sections

Increasing 2PA and ESA cross sections is important for multiphoton imaging and for many other fields. Ongoing work is focused on (1) intelligent molecular design strategies to enhance $\delta_{2PA}(\omega)$; (2) increasing the spectral range of the largest 2PA (2PA for most cyanine-like dyes have large cross sections within a relatively narrow spectral range); and (3) obtaining large ESA cross sections while maintaining long-lived excited state lifetimes, perhaps through triplet generation.

In order to determine the structural factors maximizing 2PA cross section values, we analyze (8) from Sect. 1.2.1. For all cyanine-like molecules, symmetrical and asymmetrical, several distinct 2PA bands can be measured. *First*, the less intensive 2PA band is always connected with two-photon excitation into the main absorption band. The character of this 2PA band involves at least two dipole moments, μ_{01} and $\Delta\mu$. It is well-known that 2PA into the S_1 band is symmetry forbidden for centrosymmetrical molecules, such as squaraines with C_i symmetry due to $\Delta\mu = 0$, and only slightly allowed for polymethine dyes with C_{2v} symmetry ($\Delta\mu$ is small and oriented nearly perpendicular to μ_{01}). It is important to note that a change in the permanent dipole moment under two-photon excitation into the linear absorption peak, even for asymmetrical D–π–A molecules, typically does not lead to the appearance of a 2PA band. 2PA bands under the main absorption peak are typically observed only for strongly asymmetrical molecules, for example, Styryl 1 [83], whose $S_0 \rightarrow S_1$ transitions are considerably different from the corresponding transitions in symmetrical dyes and represent much broader, less intense, and blue-shifted bands. Thus, for typical cyanine-like molecules, both symmetrical and asymmetrical, with strong and relatively narrow $S_0 \rightarrow S_1$ transitions, we observe the first 2PA band occurring at an energy shifted to the "blue" range at $\approx$1,000–1,200 cm^{-1} as compared to the peak of the $S_0 \rightarrow S_1$ transition. The 2PA final state in this case corresponds to vibrational levels of S_1. In conclusion, the nature of the first 2PA band can be attributed to the coupling between the first excited electronic state S_1 and its vibrational modes.

Second, we analyze the nature of the next, strong 2PA bands. The positions of their final states correspond to one-photon symmetry forbidden bands and can be found from excitation anisotropy measurements, as illustrated in Figs. 6, 19, and 23. Excitation anisotropy spectra for all cyanine-like molecules typically reveal a large alternation of maximum and minimum features suggesting the positions of the 1PA and 2PA transitions. Two-photon excitation into final states involves two dipole moments, μ_{01} and μ_{1fi}.

Finally, we formulate the following general trends in structure–property relations:

1. An increase of 2PA cross section can be achieved by increasing μ_{01}, which can be realized upon lengthening of the polymethine chromophore. For linear conjugated molecules, molar absorbance can be as large as 100,000–300,000 M^{-1} cm^{-1}, which corresponds to $S_0 \rightarrow S_1$ transition dipole moments of μ_{01} = 12–18 D. Note that lengthening of the conjugation chain leads to an increase of δ_{2PA} for all 2PA bands. The limitation of this factor is connected with the saturation of μ_{01}

values for the long molecules absorbing in the range ≈1,000 nm due to the ground state symmetry breaking effect discussed in Sect. 3.1. An example is shown in Fig. 14 for a series of symmetrical D–π–D polymethine dyes with trimethylindolin donor terminal groups.

2. An increase of 2PA cross section can be achieved by increasing μ_{1f}, which can be realized by introduction of a strong acceptor group into the conjugated bridge leading to a quadrupolar type arrangement D–π–A–π–D (squaraine and tetraone structures). This arrangement stimulates an effective charge transfer processes over a large distance (extended conjugation bridge) resulting in large 2PA cross section values (up to 30,000 GM [87]). Examples are shown in Fig. 18 for PD 2630, SD 2243, and TD 2765 with the same D terminal groups and similar conjugation length. As seen, considerably larger δ_{2PA} can be accessed in SD and especially in TD molecules due to the effective charge transfer transitions allowed in 2PA processes.
3. An increase of 2PA cross section can be achieved by decreasing the detuning energy $(\hbar\omega_{eg}–\hbar\omega)$ leading to ISRE (see Sect. 1.2.1). This effect can be realized in dyes with a relatively narrow absorption band with a steep edge (for example, SD, see Fig. 18) allowing the use of optical pumping at frequencies closer to the linear absorption resonance.
4. An increase of 2PA cross section can be obtained by specific arrangement of the molecular energy levels allowing for an increase of the density of final states and reaching the final states *fi* at the smallest detuning energy $(\hbar\omega_{eg}–\hbar\omega)$. This case corresponds to the so called "double resonance" condition: $\hbar\omega \rightarrow \hbar\omega_{eg}$ and $2\hbar\omega \rightarrow \omega_{e'g}$ (see Sect. 1.2.1), and is realized in SD molecules due to the increased density of final states [88].
5. An increase of 2PA cross section can be achieved in asymmetrical molecules with the proper choice of solvent polarity [86]. The main idea here is connected with the strong effect of solvent polarity on the position of the linear absorption peak $S_0 \rightarrow S_1$ but much smaller influence on the position of the 2PA band. This case is illustrated in Fig. 24 for the D–π–A dye G188. The position of the second 2PA band for this dye remains unshifted in solvents of different polarity, ACN and toluene, in spite of the large solvatochomic shift of the linear absorption band $S_0 \rightarrow S_1$. This effect leads to a large ISRE in ACN, allowing tuning closer to resonance and results in more than a two times larger δ_{2PA} in this solvent, δ_{2PA} ≈10,000 GM (≈4,700 GM in toluene). The first 2PA band follows the solvatochromic shift of the linear absorption peak and exhibits a smaller difference in 2PA cross sections: δ_{2PA} ≈1,150 GM in ACN and ≈850 GM in toluene.

4 Conclusions and Future Directions

Much of the work presented in this chapter represents a synergistic effort from several complementary research fields: quantum-chemical theory, chemical synthesis, and nonlinear optical materials characterization. This combination of expertise

is essential in order to make progress in a meaningful and directed way. Obtaining the nonlinear spectrum of a single molecule has limited value. What is needed is a large database of molecular nonlinear optical studies on several series of molecules having well-controlled differences. These differences, often small, can give trends in properties that are crucial to understanding the underlying physics that produces nonlinear absorption. Having the knowledge to be able to separate various nonlinear effects and their temporal response is also essential so as to not confuse trends. Understanding the quantum mechanical molecular states that ultimately lead to the observed nonlinear response is the final test of success in predicting nonlinear properties.

The discussion in this chapter is limited to cyanine-like NIR conjugated molecules, and further, is limited to discussing their two-photon absorption spectra with little emphasis on their excited state absorption properties. In principle, if the quantum mechanical states are known, the ultrafast nonlinear refraction may also be determined, but that is outside the scope of this chapter. The extent to which the results discussed here can be transferred to describe the nonlinear optical properties of other classes of molecules is debatable, but there are certain results that are clear. *Designing molecules with large transition dipole moments that take advantage of* intermediate state resonance *and "*double resonance*" enhancements are definitely important approaches to obtain large two-photon absorption cross sections.*

The results of this research combined with a growing literature on structure–property relations in organic materials is moving us closer to the ultimate goal of developing a predictive capability for the nonlinear optical properties of molecules; however, there is still a long way to go. Progress is slow due to the difficulties of synthesis (and the time it takes), the inadequacies of models (and the capacity of computers), and the nearly infinite variety of possible molecular structures. Of course, this last difficulty is what makes organic materials so interesting! If we do obtain a predictive capability for molecular properties, there will still be questions of what happens in the solid-state/neat materials due to strong molecular interactions, although progress is also being made in this field [89].

When we do have a good grasp of the ultimate possibilities and limits on the two-photon absorption along with the nonlinear refraction, we should have a much better understanding on what is possible to do with these nonlinear materials, i.e., what possible applications are practical and what devices can be made. On the other hand, as has been found with linear optical properties, it is often that other properties including processability, longevity, cost, and extrinsic properties that ultimately demand what material is used for a given application. Although the goal of practical molecular-based nonlinear optical devices remains mostly a hope, the continued progress in this field brings it closer to realization.

References

1. Pawlicki M, Collins HA, Denning RG, Anderson HL (2009) Two-photon absorption and the design of two-photon dyes. Angew Chem Int Ed Engl 48:3244–3266
2. Zipfel WR, Williams RM, Webb WW (2003) Nonlinear magic: multiphoton microscopy in the biosciences. Nat Biotechnol 21:1369–1377

3. Williams RM, Piston DW, Webb WW (1994) Two-photon molecular excitation provides intrinsic 3-dimensional resolution for laser-based microscopy and microphotochemistry. FASEB J 8:804–813
4. So PT, Dong CY, Masters BR, Berland KM (2000) Two-photon excitation fluorescence microscopy. Annu Rev Biomed Eng 2:399–429
5. Piston DW (1999) Imaging living cells and tissues by two-photon excitation microscopy. Trends Cell Biol 9:66–69
6. König K (2000) Multiphoton microscopy in life sciences. J Microsc 200:83–104
7. Diaspro A, Robello M (2000) Two-photon excitation of fluorescence for three-dimensional optical imaging of biological structures. J Photochem Photobiol B 55:1–8
8. Rubart M (2004) Two-photon microscopy of cells and tissue. Circ Res 95:1154–1166
9. Diaspro A, Chirico G, Federici F, Cannone F, Beretta S, Robello M (2001) Two-photon microscopy and spectroscopy based on a compact confocal scanning head. J Biomed Opt 6:300–310
10. Scherschel JA, Rubart M (2008) Cardiovascular imaging using two-photon microscopy. Microsc Microanal 14:492–506
11. Bates M, Huang B, Zhuang X (2008) Super-resolution microscopy by nanoscale localization of photo-switchable fluorescent probes. Curr Opin Chem Biol 12:505–514
12. Maria GoeppertMayer Biography http://nobelprize.org/nobel_prizes/physics/laureates/1963/mayer-bio.html
13. Goeppert-Mayer M (1931) Uber elementarakte mit zwei quantensprungen. Ann Phys 401:273–294
14. Denk W, Strickler JH, Webb WW (1990) Two-photon laser scanning fluorescence microscopy. Science 248:73–76
15. He GS, Tan LS, Zheng Q, Prasad PN (2008) Multiphoton absorbing materials: molecular designs, characterizations, and applications. Chem Rev 108:1245–1330
16. Reinhardt BA, Brott LL, Clarson SJ, Dillard AG, Bhatt JC, Kannan R, Yuan L, He GS, Prasad PN (1998) Highly active two-photon dyes: design, synthesis, and characterization toward application. Chem Mater 10:1863–1874
17. Terenziani F, D'Avino G, Painelli A (2007) Multichromophores for nonlinear optics: designing the material properties by electrostatic interactions. Chemphyschem 8:2433–2444
18. Bhawalkar JD, He GS, Prasad PN (1996) Nonlinear multiphoton processes in organic and polymeric materials. Rep Prog Phys 59:1041–1070
19. Albota M, Beljonne D, Bredas JL, Ehrlich JE, Fu JF, Heikal AA, Hess SE, Kogej T, Levin MD, Marder SR, McCord-Maughon D, Perry JW, Röckel H, Rumi M, Subramaniam G, Webb WW, Wu XL, Xu C (1998) Design of organic molecules with large two-photon absorption cross sections. Science 281:1653–1656
20. Corredor CC, Huang Z, Belfield KD (2006) Two-photon 3D optical data storage via fluorescence modulation of an efficient fluorene dye by a photochromic diarylethene. Adv Mater 18:2910–2914
21. Cumpston BH, Ananthavel SP, Barlow S, Dyer DL, Ehrlich JE, Erskine LL, Heikal AA, Kuebler SM, Lee IS, McCord-Maughon D, Qin J, Röckel H, Rumi M, Wu XL, Marder SR, Perry JW (1999) Two-photon polymerization initiators for three-dimensional optical data storage and microfabrication. Nature 398:51–54
22. Kuebler SM, Rumi M (2004) Nonlinear optics - applications: three-dimensional microfabrication. In: Guenther RD, Steel DG, Bayvel L (eds) Encyclopedia of modern optics. Oxford, Elsevier
23. Picot A, D'Aléo A, Baldeck PL, Grichine A, Duperray A, Andraud C, Maury O (2008) Long-lived two-photon excited luminescence of water-soluble europium complex: applications in biological imaging using two-photon scanning microscopy. J Am Chem Soc 130:1532–1533
24. Briñas RP, Troxler T, Hochstrasser RM, Vinogradov SA (2005) Phosphorescent oxygen sensor with dendritic protection and two-photon absorbing antenna. J Am Chem Soc 127:11851–11862

25. Kim S, Ohulchanskyy TY, Pudavar HE, Pandey RK, Prasad PN (2007) Organically modified silica nanoparticles co-encapsulating photosensitizing drug and aggregation-enhanced two-photon absorbing fluorescent dye aggregates for two-photon photodynamic therapy. J Am Chem Soc 129:2669–2675
26. Ogawa K, Kobuke Y (2008) Recent advances in two-photon photodynamic therapy. Anticancer Agents Med Chem 8:269–279
27. Ogawa K, Kobuke Y (2009) Design of two-photon absorbing materials for molecular optical memory and photodynamic therapy. Org Biomol Chem 7:2241–2246
28. Sutherland RL (1996) Handbook of nonlinear optics. Marcel Dekker, New York
29. Sheik-Bahae M, Hutchings DC, Hagan DJ, Van Stryland EW (1991) Dispersion of bound electronic nonlinear refraction in solids. IEEE J Quantum Electron 27:1296–1309
30. Hutchings DC, Van Stryland EW (1992) Nondegenerate 2-photon absorption in zinc-blend semiconductors. J Opt Soc Am B 9:2065–2074
31. Sheik-Bahae M, Wang J, Van Stryland EW (1994) Nondegenerate optical Kerr-effect in semiconductors. IEEE J Quantum Electron 30:249–255
32. Hales JM, Hagan DJ, Van Stryland EW, Schafer KJ, Morales AR, Belfield KD, Pacher P, Kwon O, Bredas JL (2004) Resonant enhancement of two-photon absorption in substituted fluorine molecules. J Chem Phys 121:3152–3160
33. Orr BJ, Ward JF (1971) Perturbation theory of the non-linear optical polarization of an isolated system. Mol Phys 20:513–526
34. Dirk CW, Cheng L, Kuzyk MG (1992) A simplified three-level model describing the molecular third-order nonlinear optical susceptibility. Int J Quantum Chem 43:27–36
35. Kuzyk MG, Dirk CW (1990) Effects of centrosymmetry on the nonresonant electronic third-order nonlinear optical susceptibility. Phys Rev A 41:5098–5109
36. Birge RR, Pierce BM (1979) A theoretical analysis of two-photon properties of linear polyenes and the visual chromophores. J Chem Phys 70:165–178
37. Cronstrand P, Luo Y, Agren H (2002) Generated few-state models for two-photon absorption of conjugated molecules. Chem Phys Lett 352:262–269
38. Monson PR, McClain WM (1970) Polarization dependence of the two-photon absorption of tumbling molecules with application to liquid 1-chloronaphthalene and benzene. J Chem Phys 53:29–37
39. Kamada K, Ohta K, Iwase Y, Kondo K (2003) Two-photon absorption properties of symmetric substituted diacetylene: drastic enhancement of the cross section near the one-photon absorption peak. Chem Phys Lett 372:386–393
40. Ohta K, Kamada K (2006) Theoretical investigation of two-photon absorption allowed excited states in symmetrically substituted diacetylenes by ab initio molecular-orbital method. J Chem Phys 124:124303
41. Lakowicz JR (1999) Principle of fluorescence spectroscopy, 2nd edn. Kluwer Academic/Plenum, New York
42. Ramakrishna G, Goodson T III, Rogers-Haley JE, Cooper TM, McLean DG, Urbas A (2009) Ultrafast intersystem crossing: excited state dynamics of platinum acetylide complexes. J Phys Chem C 113:1060–1066
43. Kleinschmidt J, Rentsch S, Tottleben W, Wilhelmi B (1974) Measurement of strong nonlinear absorption in stilbene-chloroform solutions, explained by the superposition of two-photon absorption and one-photon absorption from the excited state. Chem Phys Lett 24:133–135
44. Kannan R, He GS, Lin TC, Prasad PN, Vaia RA, Tan LS (2004) Toward highly active two-photon absorbing liquids. Synthesis and characterization of 1, 3, 5-triazine-based octupolar molecules. Chem Mater 16:185–194
45. Ehrlich JE, Wu XL, Lee IS, Hu ZY, Röckel H, Marder SR, Perry JW (1997) Two-photon absorption and broadband optical limiting with bis-donor stilbenes. Opt Lett 22:1843–1845
46. Webster S, Odom SA, Padilha LA, Przhonska OV, Peceli D, Hu H, Nootz G, Kachkovski AD, Matichak J, Barlow S, Anderson HL, Marder SR, Hagan DJ, Van Stryland EW (2009) Linear and nonlinear spectroscopy of a porphyrin-squaraine-porphyrin conjugated system. J Phys Chem B 113:14854–14867

47. Sutherland RL, Brant MC, Heinrichs J, Rogers JE, Slagle JE, McLean DG, Fleitz PA (2005) Excited-state characterization and effective three-photon absorption model of two-photon-induced excited-state absorption in organic push-pull charge-transfer chromophores. J Opt Soc Am B 22:1939–1948
48. Mishra A, Behera RK, Behera PK, Mishra BK, Behera GB (2000) Cyanines during the 1990s: a review. Chem Rev 100:1973–2012
49. Fabian J, Nakazumi H, Matsuoka M (1992) Near-infrared absorbing dyes. Chem Rev 92:1197–1226
50. Peyghambarian N, Dalton L, Jen A, Kippelen B, Marder S, Norwood R, Perry J (2006) Technological advances brighten horizons for organic nonlinear optics. Laser Focus World 42:85–94
51. Daehne S (1978) Color and constitution: one hundred years of research. Science 199:1163–1167
52. Meyers F, Marder SR, Pierce BM, Bredas JL (1994) Electric field modulated nonlinear optical properties of donor-acceptor polyenes: sum-over-states investigation of the relationship between molecular polarizabilities (α, β, and γ) and bond length alternation. J Am Chem Soc 116:10703–10714
53. Beverina L, Fu J, Leclercq A, Zojer E, Pacher P, Barlow S, Van Stryland EW, Hagan DJ, Brédas JL, Marder SR (2005) Two-photon absorption at telecommunications wavelengths in a dipolar chromophore with a pyrrole auxiliary donor and thiazole auxiliary acceptor. J Am Chem Soc 127:7282–7283
54. Hales JM, Zheng S, Barlow S, Marder SR, Perry JW (2006) Bisdioxaborine polymethines with large third-order nonlinearities for all-optical signal processing. J Am Chem Soc 128:11362–11363
55. Fisher JAN, Susumu K, Therien MJ, Yodh AG (2009) One- and two-photon absorption of highly conjugated multiporphyrin systems in the two-photon Soret transition region. J Chem Phys 130:134506
56. Eaton DF (1988) Reference materials for fluorescence measurement. Pure Appl Chem 60:1107–1114
57. Webster S, Padilha LA, Hu H, Przhonska OV, Hagan DJ, Van Stryland EW, Bondar MV, Davydenko IG, Slominsky YL, Kachkovski AD (2008) Structure and linear spectroscopic properties of near IR polymethine dyes. J Lumin 128:1927–1936
58. Gerasov AO, Shandura MP, Kovtun YP (2008) Series of polymethine dyes derived from 2, 2-difluoro-1, 3, 2-(2H)-dioxaborine of 3-acetyl-7-diethylamino-4-hydroxycoumarin. Dyes Pigm 77:598–607
59. Padilha LA, Webster S, Przhonska OV, Hu H, Peceli D, Ensley TR, Bondar MV, Gerasov AO, Kovtun YP, Shandura MP, Kachkovski AD, Hagan DJ, Van Stryland EW (2010) Efficient two-photon absorbing acceptor-π-acceptor polymethine dyes. J Phys Chem A, Submitted
60. Strickler SJ, Berg RA (1962) Relationship between absorption intensity and fluorescence lifetime of molecules. J Chem Phys 37:814–822
61. Negres RA, Przhonska OV, Hagan DJ, Van Stryland EW, Bondar MV, Slominsky YL, Kachkovski AD (2001) The nature of excited-state absorption in polymethine and squarylium molecules. IEEE J Sel Top Quantum Electron 7:849–863
62. Webster S, Fu J, Padilha LA, Przhonska OV, Hagan DJ, Van Stryland EW, Bondar MV, Slominsky YL, Kachkovski AD (2008) Comparison of nonlinear absorption in three similar dyes: polymethine, squaraine, and tetraone. Chem Phys 348:143–151
63. Lessing HE, Von Jena A (1976) Separation of rotational diffusion and level kinetics in transient absorption spectroscopy. Chem Phys Lett 42:213–217
64. Sheik Bahae M, Said AA, Van Stryland EW (1989) High-sensitivity, single beam n2 measurements. Opt Lett 14:955–957
65. Sheik-Bahae M, Said AA, Wei TH, Hagan DJ, Van Stryland EW (2007) Special 30th anniversary feature: sensitive measurement of optical nonlinearities using a single beam. IEEE LEOS Newslett 21:17–35

66. Sheik-Bahae M, Said AA, Hagan DJ, Van Stryland EW (1990) Sensitive measurement of optical nonlinearities using a single beam. IEEE J Quantum Electron 26:760–769
67. Johnston TF (1998) Beam propagation (M^2) measurement made as easy as it gets: the four-cuts method. Appl Opt 37:4840–4850
68. Firester AH, Heller ME, Sheng P (1977) Knife-edge scanning measurements of subwavelength focused light beams. Appl Opt 16:1971–1974
69. Weber HP (1967) Method for pulsewidth measurement of ultrashort light pulses generated by phase-locked lasers using nonlinear optics. J Appl Phys 38:2231–2234
70. Diels JC, Rudolph W (1996) Ultrashort laser pulse phenomena: fundamentals, techniques, and applications on a femtosecond time scale. Academic, San Diego CA, pp 365–399
71. Balu M, Hales J, Hagan DJ, Van Stryland EW (2005) Dispersion of nonlinear refraction and two-photon absorption using a white-light continuum Z-scan. Opt Express 13: 3594–3599
72. Balu M, Padilha LA, Hagan DJ, Van Stryland EW, Yao S, Belfield K, Zheng S, Barlow S, Marder S (2008) Broadband Z-scan characterization using a high-spectral-irradiance, high-quality supercontinuum. J Opt Soc Am B 25:159–165
73. Webster S, Padilha L, Przhonska O, Peceli D, Hu H, Slominsky Y, Kachkovski A, Tolmachov A, Kurdyukov V, Hagan D, Van Stryland E (2009) Enhancement of triplet yields in cyanine-like molecules. Laser Science XXV, OSA Technical Digest (CD) paper: LSTuG2
74. Santos PF, Reis LV, Duarte I, Serrano JP, Almeida P, Oliveira AS, Vieira Ferreira LF (2005) Synthesis and photochemical evaluation of iodinated squarylium cyanine dyes. Helv Chim Acta 88:1135–1143
75. Lim JH, Przhonska OV, Khodia S, Yang S, Ross TS, Hagan DJ, Van Stryland EW, Bondar MV, Slominsky YL (1999) Polymethine and squarylium molecules with large excited-state absorption. Chem Phys 245:79–97
76. Kaiser W, Garrett CGB (1961) Two-photon excitation in CaF_2:Eu^{2+}. Phys Rev Lett 7:229–231
77. Xu C, Webb WW (1996) Measurement of two-photon excitation cross sections of molecular fluorophores with data from 690 to 1050 nm. J Opt Soc Am B 13:481–491
78. Padilha LA, Webster S, Hu H, Przhonska OV, Hagan DJ, Van Stryland EW, Bondar MV, Davydenko IG, Slominsky YL, Kachkovski AD (2008) Excited state absorption and decay kinetics of near IR polymethine dyes. Chem Phys 352:97–105
79. Iordanov TD, Davis JL, Masunov AE, Levenson A, Przhonska OV, Kachkovski AD (2009) Symmetry breaking in cationic polymethine dyes, part 1: ground state potential energy surfaces and solvent effects on electronic spectra of streptocyanines. Int J Quantum Chem 109:3592–3601
80. Ryabitsky AB, Kachkovski AD, Przhonska OV (2007) Symmetry breaking in cationic and anionic polymethine dyes. J Mol Struct-Theochem 802:75–83
81. Lepkowicz RS, Przhonska OV, Hales JM, Fu J, Hagan DJ, Van Stryland EW, Bondar MV, Slominsky YL, Kachkovski AD (2004) Nature of the electronic transitions in thiacarbocyanines with a long polymethine chain. Chem Phys 305:259–270
82. Su WP, Schrieffer JR, Heeger AJ (1979) Soliton in polyacetylene. Phys Rev Lett 42:1698–1701
83. Fu J, Padilha LA, Hagan DJ, Van Stryland EW, Przhonska OV, Bondar MV, Slominsky YL, Kachkovski AD (2007) Molecular structure – two-photon absorption property relations in polymethine dyes. J Opt Soc Am B 24:56–66
84. Luo Y, Norman P, Macak P, Ågren H (2000) Solvent-induced two-photon absorption of a push − pull molecule. J Phys Chem A 104:4718–4722
85. Terenziani F, Katan C, Badaeva E, Tretiak S, Blanchard-Desce M (2008) Enhanced two-photon absorption of organic chromophores: theoretical and experimental assessments. Adv Mater 20:4641–4678
86. Padilha LA, Webster S, Przhonska OV, Hu H, Peceli D, Rosch JL, Bondar MV, Gerasov AO, Kovtun YP, Shandura MP, Kachkovski AD, Hagan DJ, Van Stryland EW (2009) Nonlinear

absorption in a series of donor–π–acceptor cyanines with different conjugation lengths. J Mater Chem 19:7503–7513
87. Chung SJ, Zheng S, Odani T, Beverina L, Fu J, Padilha LA, Biesso A, Hales JM, Zhan X, Schmidt K, Ye A, Zojer E, Barlow S, Hagan DJ, Van Stryland EW, Yi Y, Shuai Z, Pagani GA, Brédas JL, Perry JW, Marder SR (2006) Extended squaraine dyes with large two-photon absorption cross-sections. J Am Chem Soc 128:14444–14445
88. Fu J, Padilha LA, Hagan DJ, Van Stryland EW, Przhonska OV, Bondar MV, Slominsky YL, Kachkovski AD (2007) Experimental and theoretical approaches to understanding two-photon absorption spectra in polymethine and squaraine molecules. J Opt Soc Am B 24:67–76
89. Hu H, Gerasov AO, Padilha LA, Przhonska OV, Webster S, Shandura MP, Kovtun YP, Masunov AE, Hagan DJ, Van Stryland EW (2010) Two-photon absorption in single crystals of cyanine-like dye. CLEO/QELS 2010, San Jose CA, Submitted